Unique ocean circulation pathways reshape the Indian Ocean oxygen minimum zone with warming

Sam Ditkovsky[1], Laure Resplandy[2], and Julius Busecke[3]

[1]Program in Atmospheric and Oceanic Sciences, Princeton University, Princeton, NJ, USA
[2]Department of Geosciences and High Meadows Environmental Institute, Princeton University, Princeton, NJ, USA
[3]Lamont-Doherty Earth Observatory, Columbia University, New York, NY, USA

Correspondence: Sam Ditkovsky (samjd@princeton.edu)

Abstract. The global ocean is losing oxygen with warming. Observations and Earth system model projections suggest, however, that this global ocean deoxygenation does not equate to a simple and systematic expansion of tropical oxygen minimum zones (OMZs). Previous studies have focused on the Pacific Ocean; they showed that the outer OMZ deoxygenates and expands as oxygen supply by advective transport weakens, the OMZ core oxygenates and contracts due to a shift in the composition of the source waters supplied by slow mixing, and in between these two regimes, oxygen is redistributed with little effect on OMZ volume. Here, we examine the OMZ response to warming in the Indian Ocean using an ensemble of Earth system model high-emissions scenario experiments from the Coupled Model Intercomparison Project phase 6. We find a similar expansion-redistribution-contraction response, but show that the unique ocean circulation pathways of the Indian Ocean leads to far more prominent OMZ contraction and redistribution regimes than in the Pacific Ocean. As a result, only the outermost ~~OMZ layers~~ volumes (oxygen $> 180 \, \mu\mathrm{mol/kg}$) expand. The Indian Ocean experiences a broad oxygenation in the southwest driven by a reduction in waters supplied by the Indonesian Throughflow in favor of high-oxygen waters supplied from the South Indian Gyre. Models also project a strong localized deoxygenation in the northern Arabian Sea due to the rapid warming and shoaling of marginal sea outflows (Red Sea and Persian Gulf), and increases in local stratification with warming. We extend the existing conceptual framework used to explain the Pacific OMZ response to interpret the response in the Indian Ocean.

1 Introduction

Oxygen minimum zones (OMZs) are naturally occurring low-oxygen regions located in subsurface tropical oceans (typically 100-1500 m). OMZs develop in the "shadow zones" of the ocean thermocline where oxygen supply by ocean circulation is weak (Luyten et al., 1983; Pedlosky, 1983), and are generally located below highly productive surface systems that boost respiration and biological oxygen demand at the subsurface (Paulmier and Ruiz-Pino, 2009). The global ocean has lost oxygen in response to global warming (Keeling et al., 2010; Helm et al., 2011; Schmidtko et al., 2017; Bindoff et al., 2019), and this trend is expected to continue and accelerate over the twenty-first century if anthropogenic emissions are not significantly drawn

down (Bopp et al., 2013; Kwiatkowski et al., 2020). Global deoxygenation has been attributed to weakening ocean ventilation (i.e., weakening oxygen supply by ocean circulation and mixing) and decreasing oxygen solubility in seawater with warming (e.g., Oschlies et al., 2018). A concern is that OMZs are expanding in response to global deoxygenation, potentially disrupting the physiology and survival of marine organisms and compressing the habitats of marine species requiring oxygen for their survival (Vaquer-Sunyer and Duarte, 2008; Miller et al., 2002; Stramma et al., 2008, 2012; Deutsch et al., 2020; Levin, 2018). The fate of OMZs under warming, in particular the two most intense regions found in the tropical Pacific Ocean and tropical Indian Ocean, has however been highly debated, with apparently inconsistent changes found across hydrographic observations, paleo-oceanographic proxies and Earth system model (ESM) projections. In-situ hydrographic observations collected since the 1950s suggest that the tropical Indo-Pacific Oceans and the marginal seas that supply oxygen to the tropical Indian Ocean (including the Persian Gulf and Red Sea) have lost oxygen, supporting the view that tropical OMZs are expanding (Stramma et al., 2008; Helm et al., 2011; Ito et al., 2017; Banse et al., 2014; Piontkovski and Al-Oufi, 2015; Queste et al., 2018; Naqvi, 2021). Yet, paleo-oceanographic studies suggest that the OMZ in the eastern tropical Pacific Ocean has contracted, rather than expanded, under past warming conditions (Deutsch et al., 2014; Auderset et al., 2022). Looking into the future, studies using ESM ensembles have projected a robust deoxygenation at mid- and high-latitudes with warming, consistent with the weakening of ventilation found at the global scale, but have failed, until recently, to reach a consensus on the expected changes in oxygen and OMZ volumes in tropical oceans (Cocco et al., 2013; Bopp et al., 2013; Cabré et al., 2015; Bopp et al., 2017; Resplandy, 2018; Kwiatkowski et al., 2020).

Busecke et al. (2022) recently showed that the inconsistencies found in the fate of the OMZ in the Pacific Ocean could be reconciled using an ensemble of ESMs from the Coupled Model Intercomparison Project Phase 6 (CMIP6; Eyring et al., 2016). They found that the OMZ response to global warming was in fact consistent across the ESMs when examined in an oxygen-space framework and fell into three regimes: an expansion of the OMZ outer layers (large OMZ volume delimited by oxygen thresholds of typically $\sim100\,\mu\mathrm{mol/kg}$ or higher), a contraction of the eastern Pacific "OMZ core" waters (OMZ volume delimited by oxygen thresholds of $\sim20\,\mu\mathrm{mol/kg}$ or lower), and a "transition regime" between contraction and expansion that experiences weak and uncertain changes associated with a spatial redistribution of the OMZ volume. This three-regime framework reconciles hydrographic work that show an OMZ expansion in the central Pacific Ocean where the OMZ outer layers are located (Stramma et al., 2008), and paleo-oceanographic studies that found evidence for a contraction in the eastern Pacific (note that these studies used nitrogen isotopes which are a proxy for "OMZ core" denitrifying waters; Deutsch et al., 2014; Auderset et al., 2022). The framework also explains the discrepancies found in previous modeling studies that often considered OMZ volume definitions that fall in the transition regime where changes are smaller and uncertain (e.g., Bopp et al., 2013; Cabré et al., 2015). In the Pacific Ocean, the apparent discrepancy between outer OMZ expansion and core contraction can be interpreted using the conceptual framework proposed by Gnanadesikan et al. (2007), which distinguishes between two models of ocean ventilation: (1) a "single-pipe" model where ventilation is controlled by advection from one source water mass, and (2) a "mixing-network" model in which ventilation rates are sustained by slow mixing of multiple source waters as in ocean shadow zones (Lévy et al., 2022; Gnanadesikan et al., 2013; Brandt et al., 2015). As ocean circulation pathways weaken, regions ventilated by a single-pipe experience reduced supply of oxygen (transport rates of oxygenated surface water to the

2

thermocline slows), while regions ventilated by a mixing-network can either experience a reduction or increase in ventilation and oxygen supply (by changing the connectivity and the contributions of each source water to the mixing-network). The single-pipe model explains the deoxygenation of the outer OMZ layers, which has been attributed to the weakening of the northern and southern subtropical cells that ventilate the outer layers of the OMZ (Gnanadesikan et al., 2012; Duteil et al., 2014; Busecke et al., 2022; Duteil et al., 2021; Llanillo et al., 2018; Margolskee et al., 2019). In contrast, changes in mixing-network connectivity explain the oxygenation of the Pacific OMZ core, which was attributed to reduced contributions from aged, oxygen-poor deep and intermediate waters, shifting the mixing ratio towards younger, oxygen-rich upper ocean waters (Bryan et al., 2006; Gnanadesikan et al., 2007, 2012; Takano et al., 2018; Busecke et al., 2022).

The fate of the Indian Ocean OMZ has been far less studied than its Pacific Ocean counterpart. Yet, the Indian Ocean shows some of the fastest ocean warming trends in the world (Roxy et al., 2014; Sharma et al., 2023), and the expansion of its OMZ could have detrimental effects for coastal populations that depend heavily on marine resources for food security and economic stability in the region (Bouchard and Crumplin, 2010; Clifton et al., 2012; Gattuso et al., 2015; Llewellyn et al., 2016; Roy, 2019). The ventilation pathways and OMZ geometry in the Indian Ocean are fundamentally different from the two subtropical cells (one in each hemisphere) and eastern boundary OMZ found in the Pacific Ocean. It is thus unclear whether the "single-pipe and mixing-network" framework which characterizes the Pacific Ocean is sufficient to describe the behavior of the Indian Ocean. The Indian Ocean is bounded by continent to the north and ventilation is almost exclusively sustained by one subtropical cell originating in the South Indian Gyre (Harper, 2000; Schott et al., 2002; Phillips et al., 2021). As a result, oxygen levels are higher in the southern Indian Ocean while an OMZ extends over most of the Arabian Sea and the Bay of Bengal in the north (see ~~Figure~~ Fig. 1 for observed climatological oxygen field and major ventilation pathways). Other peculiarities of the Indian Ocean ventilation are the Indonesian Throughflow which brings waters from the tropical Pacific Ocean into the Southern Indian Ocean (Sprintall et al., 2009), and the saline marginal sea outflow waters from the Red Sea and Persian Gulf that ventilate the Arabian Sea (Rhein et al., 1997; Beal et al., 2000; Menezes, 2021; Sheehan et al., 2020). Ventilation by all these advective pathways (Southern Gyre, Indonesian Throughflow and marginal seas) is projected to weaken in response to climate change (Sen Gupta et al., 2016; Feng et al., 2017; Stellema et al., 2019; Lachkar et al., 2019; Kobayashi et al., 2012), but the extent to which these changes in ventilation will affect basin-scale oxygen content and the OMZ in the Indian Ocean is however still poorly constrained. Here, we examine changes in oxygen content and OMZ volume in the Indian Ocean in response to climate change using an ensemble of CMIP6-generation ESMs with a focus on thermocline depths (upper 1000 m). We show that the fate of the Indian Ocean OMZ is consistent with the three-regime framework identified in the Pacific Ocean (Busecke et al., 2022) but that broad oxygenation results in a much more prominent contraction regime in the Indian Ocean than in the Pacific Ocean. Interpreting these changes in oxygen and OMZ volume in the Indian Ocean calls for an extension of the single-pipe and mixing-network conceptual framework to include the unique contributions from the Indonesian Throughflow and marginal seas, which we show can be interpreted as "two-pipe" and "moving-pipe" systems.

2 Methods

2.1 Datasets

We use an ensemble of ~~8~~ eight ESMs from the CMIP6 archive (Eyring et al., 2016; O'Neill et al., 2016). Out of the 14 CMIP6 ESMs that provided monthly dissolved oxygen data for the pre-industrial control, historical, and SSP5-8.5 experiments (Busecke et al., 2022), ~~5 models do not simulate an OMZ core~~ we exclude six models that simulate virtually no suboxic (≤ 10 μmol/kg) volume in the Arabian Sea (ACCESS-ESM1-5, CanESM5, CanESM5-CanOE, CNRM-ESM2-1, IPSL-CM6A-LR; ~~Fig~~ Table S1)~~, and 1 additional model has an extraordinary bias in the low oxygenated waters (CNRM-ESM2-1; Fig S2), simulating nearly double the observed volume of waters below 150 μmol/kg in the Indian Ocean~~. We keep the ~~8~~ eight remaining ESMs (GFDL-CM4, GFDL-ESM4, MIROC-ES2L, MPI-ESM1-2-HR, MPI-ESM1-2-LR, NorESM2-LM, NorESM2-MM, UKESM1-0-LL). ~~Indeed, ESMs tend to overestimate oxygen concentrations in the Arabian Sea (Oschlies et al., 2008; Bopp et al., 2013; Ri~~ ~~. A common source of this bias is unrealistically strong ventilation from the Red Sea Outflow, where the narrow outflow channel is difficult to represent on a coarse ocean grid, which results in elevated oxygen levels in~~ All six ESMs excluded from the multi-model mean exhibit above average salinity biases in the Arabian Sea~~(Schmidt et al., 2021). We find that 3 out of the 5 discarded ESMs with particularly high oxygen concentrations in the Arabian Sea (CanESM5, CanESM5-CanOE and IPSL-CM6A-LR) are characterized by annual average~~, likely from outflows (Fig. S1), and four of six models exhibit Red Sea outflow ~~rate more than double~~ rates over twice the observed rate ~~(Fig. S3; Sofianos and Johns, 2007).~~ (Fig. S2). Thus, the representation of marginal sea outflows may be improved significantly in our ensemble by excluding these ESMs. For this analysis, we use oxygen, salinity, ~~potential temperature and when available, ideal age and mass transport (7 ESMs have ideal age and~~ and potential temperature for all 8 models. When available, we also use output for ideal age (available for six ESMs), export of organic carbon at 100 m (available for seven ESMs) and mass transport (available for 5 ~~have mass transport~~ ~~). Only~~ ESMs). Stratification is calculated from potential temperature and salinity fields using the `GSW-python` package (Firing et al., 2021). To limit computational costs of this study, and because we expect inter-model variability in dissolved oxygen to dominate over internal variability, only one member is used for each model. See Table 1 for member labels and data availability of each model. All model outputs were regridded (via bilinear interpolation) to a uniform $1° \times 1°$ grid using the xESMF python package (Zhuang et al., 2021), but transport calculations were performed on each model's native grid (Sect. 2.2.4). The pre-industrial simulations were used to remove the linear control drifts from all scalar fields (oxygen, salinity, temperature, ideal age, export) in the historical and SSP5-8.5 simulations using the xMIP python package ~~to unify metadata between parent and child simulations~~ (Busecke and Spring, 2020).

We also use the observational climatology of dissolved oxygen concentrations from the World Ocean Atlas 2018 (WOA18; Garcia et al., 2019) to evaluate the representation of the Indian Ocean OMZ and dissolved oxygen field in the ensemble of ESMs. We use an average over the period of 1950-2015 in the historical simulations to compare to the observed climatology.

Table 1. ESM data used in this study. Variables used: Dissolved oxygen concentration (o2), salinity (so), potential temperature (thetao), ideal age (agessc), ~~export of organic carbon at 100 m (epc100)~~ and mass transport (umo/vmo) where available. All data used in this study is ~~publically~~ publicly available via ESGF, except ideal age fields from GFDL-CM4 and GFDL-ESM4 (see Busecke et al., 2022)

ESM	Variables	Member ID
GFDL-CM4 (Guo et al., 2018a, b)	o2, thetao, so, agessc	r1i1p1f1
GFDL-ESM4 (Krasting et al., 2018; John et al., 2018)	o2, thetao, so, agessc, epc100	r1i1p1f1
MIROC-ES2L (Hajima et al., 2019; Tachiiri et al., 2019)	o2, thetao, so, agessc, epc100	r1i1p1f2
MPI-ESM1-2-HR (Jungclaus et al., 2019; Schupfner et al., 2019)	o2, thetao, so, ~~agessc~~epc100, umo/vmo	r1i1p1f1
MPI-ESM1-2-LR (Wieners et al., 2019b, a)	o2, thetao, so, agessc, epc100, umo/vmo	r1i1p1f1
NorESM2-LM (Seland et al., 2019a, b)	o2, thetao, so, agessc, epc100, umo/vmo	r1i1p1f1
NorESM2-MM (Bentsen et al., 2019a, b)	o2, thetao, so, agessc, epc100, umo/vmo	r1i1p1f1
UKESM1-0-LL (Tang et al., 2019; Good et al., 2019)	o2, thetao, so, epc100, umo/vmo	r1i1p1f2

2.2 Analysis

To characterize the response of ocean variables to climate change, we used linear trends over the 2015-2100 period in the SSP5-8.5 simulations (normalized to change per century), except when calculating water mass ~~mixing ratios~~ fractions (Sect. 2.2.4), for which we compare historical (1950-2015 average) and end-of-century (historical plus ~~75-year trend~~ integrated linear trend over 85-years) states. To represent the ESM ensemble, we take the mean over models (multi-model mean) and use one standard deviation of the model spread on either side of the mean as a measure of uncertainty. When presenting multi-model mean trend fields, we stipple where less than 75 % of available models agree on the sign of change to indicate regions of uncertainty. While we perform our analysis over the full water column, we focus on thermocline depths (upper 1000 m) so that the results may characterize impacts on mesopelagic ecosystems. When examining oxygen and ideal age trends, we exclude surface waters by examining changes between 100 and 1000 m.

2.2.1 Tracking ocean volume by oxygen threshold

OMZ volume is generally defined as the volume of water below a chosen oxygen concentration threshold. We extend this idea to a wide range of oceanic oxygen concentration values. Here, we define the full column OMZ volume as a function of oxygen thresholds, $O_{2,T}$ (following Busecke et al., 2022):

$$\mathcal{V}_{O_2}(O_{2,T}) = \iiint_{O_2 \leq O_{2,T}} dV \tag{1}$$

where we integrate over the Indian Ocean from 30° S - 25° N and from the African continent to the west to Indonesia and Australia, extending to about 125° E in the main strait of the Indonesian Throughflow (Timor Sea), to the east. The Red Sea and Persian Gulf are not included in the integration of $\mathcal{V}_{O_2}$. We use the Equator to delimit the Arabian Sea and Bay of Bengal

sub-basins to the south. However, we do not focus on the full OMZ volume, but rather on the thermocline OMZ volume:

$$\mathcal{V}_{O_2^{1000}}(O_{2,T}) = \int\limits_{\substack{0 \\ O_2 \le O_{2,T}}}^{1000\mathrm{m}} \iint dV \tag{2}$$

Note that we integrate over the upper 1000 m here, rather than 100 to 1000 m, because OMZ volume will naturally exclude surface waters. In both cases, we use oxygen thresholds $O_{2,T}$ that vary between 5 and 225 μmol/kg and highlight ~~two~~ three benchmark thresholds: (1) $O_{2,T}$ = 20 μmol/kg (OMZ20) as the core of the OMZ, (2) $O_{2,T}$ = 60 μmol/kg (OMZ60) as a commonly cited threshold for hypoxia at which marine ecosystems tend to experience significant loss of biodiversity (Vaquer-Sunyer and Duarte, 2008), and (~~2~~3) $O_{2,T}$ = 150 μmol/kg (OMZ150) as a common habitat boundary for large commercial fish species such as tuna ~~(Brill, 1996; Prince and Goodyear, 2006; Bertrand et al., 2011; Stramma et al., 2012; Dueri et al., 2014). We also discuss changes in the OMZ core ($O_{2,T}$ = 20~~(Brill, 1996; Prince and Goodyear, 2006; Bertrand et al., 2011; Stramma et al., 2012; Dueri, 2~~. We note that oxygen thresholds above 150 μmol/kg ~~) as used in (Busecke et al., 2022)~~are not generally used to delimit low oxygen environments and OMZs, but we present them here to provide a holistic view of forced changes in oxygen distribution.

2.2.2 Thermal and non-thermal dissolved oxygen trends

We separate the influences of thermal and non-thermal processes on oxygen trends. The thermal component, or oxygen saturation O_{2SAT}, is calculated using the `GSW-python` package from potential temperature and salinity fields (Firing et al., 2021). The non-thermal component, related to ocean ventilation and biological sources and sinks of oxygen, is computed as the residual between O_2 and O_{2SAT} and is referred to as Apparent Oxygen Utilization (AOU):

$$O_2 = O_{2SAT} - \mathrm{AOU} \tag{3}$$

We compute O_{2SAT} and AOU for each year in the historical and SSP5-8.5 simulations, then take historical means and projected linear trends. Trends in $-$AOU represent the contribution of non-thermal processes to overall changes in dissolved oxygen but they encompass both changes in physical (ventilation changes tied to slower circulation or changes in mixing) and biological (respiration rates) effects. We use the ideal age of seawater (i.e., the time since exposure to the surface) to qualitatively infer the contribution of physical ventilation changes~~, and compute the Pearson Correlation Coefficients between interannual anomalies in ideal age and AOU over the SSP5-8.5 experiment (calculated with respect to a 1950-2015 mean from the historical simulations) to assess the importance of ventilation changes compared to biological changes~~.

2.2.3 ~~Quantifying~~ Identifying changes in ~~transport by~~ ventilation ~~pathways~~pathway contributions

~~To help interpret trends in dissolved oxygen and ideal age, we quantify changes in individual thermocline ventilation pathways using mass transport fields on each model's native grid. The Indonesian Throughflow Water transport is calculated as the westward flow through the main strait of the Indonesian Throughflow (the Timor Sea) integrated between 100 and 1000 m. The Southern Pathway Waters transport is calculated as the northward flow across 30°S integrated between 100 and 1000 m.~~

6

~~The upwelling of Deep Waters into the thermocline is calculated as the budget residual of transport below 1000 m across 30°S and through the main strait of the Indonesian Throughflow. Transports by marginal sea outflows from the Red Sea and Persian Gulf are defined as the outflowing components through their respective channels. We report transport trends in Sv/century, using a constant reference density of 1025 kg/m³ to convert between mass and volume transport. Transport fields are available for 5/8 ESMs in the ensemble (MPI-ESM1-2-HR, MPI-ESM1-2-LR, NorESM2-LM, NorESM2-MM, UKESM1-0-LL).~~

2.2.4 ~~**Identifying changes in water mass mixing ratios**~~

In sections 3.5 and 3.6, we solve a ~~mixing~~ mixture model in the South Equatorial Current and in the Arabian Sea to evaluate shifts in water mass ~~mixing ratios~~ fractions under SSP5-8.5 forcing. The ~~mixing~~ mixture model is based on extended Optimum Multiparameter Analysis (OMP) (Tomczak and Large, 1989; Karstensen and Tomczak, 1998). This technique solves for the ~~mixing ratios~~ water mass fractions at a given hydrographic section using the hydrographic properties of specified source water ~~masses~~ mass types (see references and Appendix A for details), _each representing an advective ventilation pathway_. We use a python implementation ~~(pyOMPA Shrikumar et al., 2022)~~ (pyOMPA; _Shrikumar et al., 2022_), based on the original MATLAB code from Karstensen and Tomczak (1998). We perform this analysis along potential density surfaces referenced to zero pressure (σ_0), calculated from potential temperature and salinity fields using the GSW-python package (Firing et al., 2021). For each region, we use a nominal value for potential density that captures features of significant dissolved oxygen change; however, we tune this value ~~slightly~~ (within 0.5) for individual ESMs to better capture features across models.

The number of source water ~~masses~~ mass types is limited to be less than or equal to the number of hydrographic properties available. Here, we use potential temperature, salinity, dissolved oxygen and AOU. To account for remineralization along the pathways (between source and case study regions), we allow for the conversion of dissolved oxygen to AOU (see Appendix A for details). In the case of the South Equatorial Current region, the source ~~waters~~ water types are Indonesian Throughflow Water, Southern Pathway Waters and Arabian Sea Water, ~~determined~~ centered at (15°S, 120°E), (30°S, 100°E) and (15°N, 65°E) respectively at a nominal potential density of $\sigma_0 = 26.4$. In the case of the Arabian Sea, the source waters are Persian Gulf Water, Red Sea Outflow Water and Arabian Sea Water ~~determined~~ centered at (24.5°N, 58.5°E), (12°N, 47°E) and (15°N, 65°E) respectively at a nominal potential density of $\sigma_0 = 25.7$. _We exclude MIROC-ES2L from the OMP analysis in the Arabian Sea because the model does not resolve the Persian Gulf and Red Sea. To account for the sensitivity of results to small changes in the sampling of source water types and potential density layer, we average 50 realizations of the experiment applying random perturbations to source water locations and density layers from their central values. Source water locations are perturbed by up to 5° in latitude and longitude for the South Equatorial Current region and 2° for the Arabian Sea. For both locations, the value of the potential density layer is perturbed by up to 0.1 kg/m³._

For each ESM in the ensemble, we solve ~~this mixing model for~~ for the water mass fractions, f, for a historical state and an end-of-century state. For the historical state, we first compute potential density for the historical mean (1950-2015) for each ESM, and use the xgcm ~~(Nicholas et al., 2023)~~ (Abernathey et al., 2022) package to transform the vertical coordinates of each model to potential density space. We note that the results of the ~~mixing model~~ OMP are not sensitive to the order of operations (temporal averaging and vertical transformation). To compute an end-of-century state, we add ~~75-year~~ 85-year

7

(2015-2100) forced trends from the SSP5-8.5 simulations to historical mean fields (potential temperature, salinity, oxygen, AOU) to represent a climatological year 2100, then repeat the coordinate transformation described above.

From the OMP results, we quantify the change in oxygen supply due to shifts in water mass composition and properties for key regions:

$$\Delta O_{2,\text{supply}} = \sum_i f_{i,1} O_{i,1} - \sum_i f_{i,0} O_{i,0} \qquad (4)$$

where f_i and O_i are the fraction and oxygen concentration of source water type i, for future (1) and historical (0) states. We compare $\Delta O_{2,\text{supply}}$ to the total simulated changes in oxygen to evaluate how well changes in the system can be described by only isopycnal transport and mixing of source water mass types. While for conservative tracers (i.e. potential temperature and salinity) the change in supply and total change should be equal if the system is well represented by the OMP analysis, an allowance for the remineralization of oxygen can lead to an imbalance between the two quantities (see Appendix A).

A concern when solving for forced trends on a potential density layer is that the results may be influenced by the displacement of this isopycnal in depth. Indeed, the potential density layers chosen here are displaced deeper in the water column by about 100 m between the historical and end-of-century states. To evaluate the impact of this deepening, we perform an alternate set of ~~mixing model~~ OMP experiments where we use a lower density value ~~to evaluate~~ at the end-of-century state than ~~used to evaluate~~ for evaluating the historical state. ~~This~~ The layer defined by this lower density value ~~is tuned to sample~~ samples the same depth as was sampled for the historical state. The results of this alternative analysis, presented in Supplementary Information, are qualitatively similar to the analysis presented in the main text, and do not change the main results.

2.2.4 Quantifying changes in transport by ventilation pathways

To provide context for trends in dissolved oxygen and ideal age, we quantify changes in individual thermocline ventilation pathways using mass transport fields on each model's native grid. The Indonesian Throughflow Water transport is calculated as the westward flow through the main strait of the Indonesian Throughflow at 114°E integrated between 100 and 1000 m. The Southern Pathway Waters transport is calculated as the northward flow across 30°S integrated between 100 and 1000 m. We note that this representation of Southern Pathway Waters largely excludes the contribution of Subtropical Underwaters, which subduct north of 30°S. The upwelling of Deep Waters into the thermocline is calculated as the budget residual of transport below 1000 m across 30°S and through the Indonesian Throughflow at 114°E. Transports by marginal sea outflows from the Red Sea and Persian Gulf are defined as the outflowing components through their respective channels. We report transport trends in Sv/century, using a constant reference density of $1025\,\text{kg/m}^3$ to convert between mass and volume transport. Transport fields are available for five of the eight ESMs in the ensemble (MPI-ESM1-2-HR, MPI-ESM1-2-LR, NorESM2-LM, NorESM2-MM, UKESM1-0-LL).
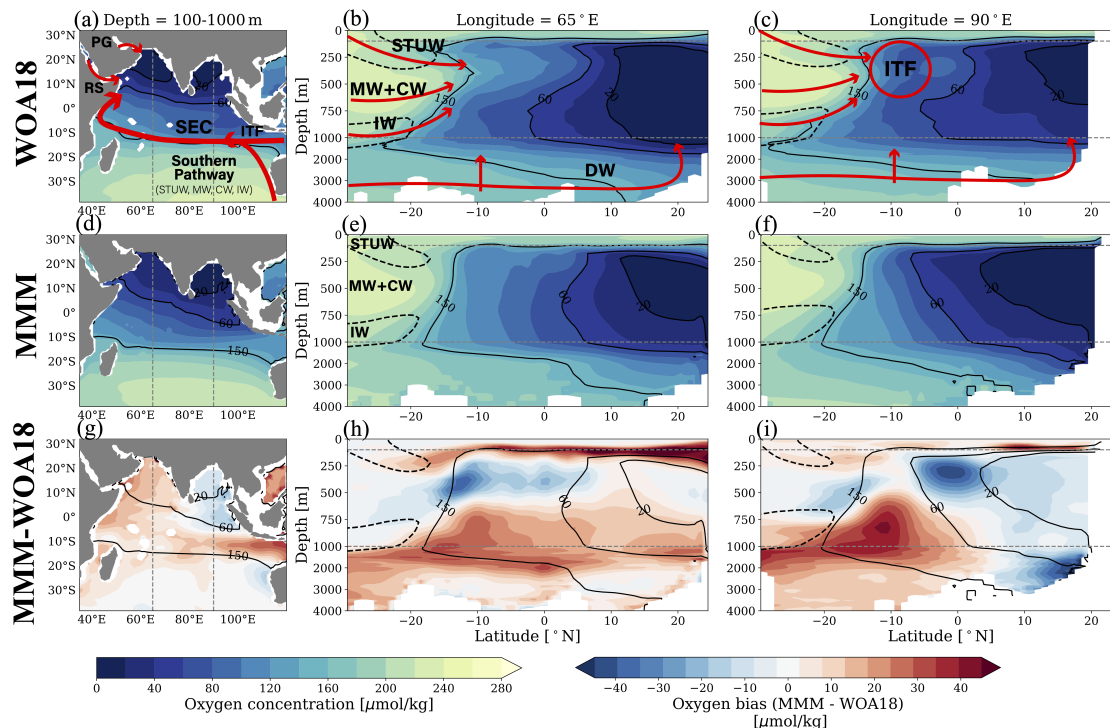
Figure 1. Dissolved oxygen annual mean climatology from World Ocean Atlas 2018 (WOA18) **(a)** averaged between 100 and 1000 m, at **(b)** 65°E and **(c)** 90°E. Multi-model mean (MMM) dissolved oxygen in the Indian Ocean for historical period (1950-2015) **(d)** between 100 and 1000 m, **(e)** at 65°E, and **(f)** at 90°E. Difference between MMM (1950-2015) and WOA18 dissolved oxygen **(g)** between 100 and 1000 m, **(h)** at 65°E, and **(i)** at 90°E. Solid black contours represent 20, 60 and 150 μmol/kg oxygen in **(a-c)** WOA18 and **(d-i)** MMM. **(a,d,g)** Dashed gray lines indicate 65°E and 90°E. **(b,c,e,f,h,i)** Dashed gray lines indicate depth of 100 and 1000 m, dashed black contours show salinity contours highlighting Subtropical Underwater and Intermediate Water. Water masses and ventilation pathways are illustrated schematically. Abreviations: South Equatorial Current (SEC), Central Water (CW), Deep Water (DW), Subtropical Underwater (STUW), Mode Water (MW), Intermediate Water (IW), Indonesian Throughflow (ITF).

3 Results

3.1 Historical oxygen and ventilation pathways in observations and Earth system models

The observed oxygen distribution in the Indian Ocean thermocline (100 to 1000 m) is influenced by five main ventilation pathways (Fig. 1a-c). First, the Southern Pathway Waters which enter via the South Indian Gyre include (from least to most dense) Subtropical Underwater (STUW; about 100 to 250 m depth), Indian Central Water and Subantarctic Mode Water (CW+MW; about 250 to 750 m depth) and Antarctic Intermediate Water (IW; about 750 to 1000 m depth) (Sprintall and Tomczak, 1993; Karstensen and Tomczak, 1997; McCarthy and Talley, 1999; Karstensen and Quadfasel, 2002; Fine, 1993; Talley, 2011). This spectrum of waters enters the basin with a range of oxygen between about 160 to 250 μmol/kg, where Indian Central Water

9

and Subantarctic Mode Water account for the highest oxygen levels. Southern Pathway Waters are capped by the salinity max-
imum of Subtropical Underwater and the salinity minimum of Antarctic Intermediate Water (dashed black contours in Fig.
1b,c). Second, the Indonesian Throughflow (ITF) brings waters from the tropical Pacific Ocean (with oxygen concentrations of
about 80-170 μmol/kg between 100 to 1000 m depth) into the Southern Indian Ocean and which mix with Southern Pathway
Waters in the South Equatorial Current (SEC). This mixture of waters then crosses the equator with the western boundary
current to ventilate the northern basin (pathway schematic in Fig. 1a) via eddy mixing, monsoonal currents and the weak North
Equatorial Current which flows east in the summer along about 5° N (Schott et al., 2009; Phillips et al., 2021; Resplandy et al.,
2012; Lachkar et al., 2016). In the northern Indian Ocean, two additional pathways are associated with saline marginal sea
outflows: Red Sea Outflow Water (RS, with concentrations around 70 μmol/kg) and Persian Gulf Water (PG, near oxygen
saturation >200 μmol/kg) deliver oxygen directly to the OMZ core in the Arabian Sea as they are ~~are~~ quickly diluted by mix-
ing (Fig. 1a). Finally, the fifth pathway corresponds to Deep Waters (DW) that enter from the Southern Ocean and Indonesian
Throughflow (here taken as waters below 1000 m depth) and slowly upwell in the basin (McCarthy et al., 1997), ventilating
the thermocline from below with relatively well oxygenated waters (100 - 200 μmol/kg).

The multi-model mean (eight ESMs, see methods) captures the main features associated with the five pathways ventilating
the Indian Ocean (Fig. 1d-f). ~~In particular, the oxygen supply by the Southern Pathway and the Indonesian Throughflow is relatively well simulated (Fig. 1a-c), with an oxygen maximum associated with Indian Central Water and Subantarctic Mode Water.~~ The multi-model mean simulates the full spectrum of Southern ~~Pathways~~ Pathway Waters, indicated by the salinity
maximum and minimum associated with Subtropical Underwater and Antarctic Intermediate Water (dashed black contours
in ~~Figure~~ Fig. 1e,f), and overall captures the temperature and salinity properties of water masses across the basin (Fig. S5).
We note that three of the eight ESMs simulate the Southern Pathway Waters particularly well (GFDL-CM4, GFDL-ESM4,
and UKESM1-0-LL), while three others are missing the salinity minimum associated with Antarctic Intermediate Water
(MIROC-ES2L, MPI-ESM1-2-HR and MPI-ESM1-2-LR, Fig. S4). ~~Overall, the~~ The oxygen supply from the Southern Pathway
and the Indonesian Throughflow is also relatively well simulated by the multi-model mean (Fig. 1a-c), and the observed oxygen
maximum associated with Indian Central Water and Subantarctic Mode Water is present in all the ESMs in the ensemble
(though it is weaker than observed in MPI-ESM1-2-HR and MPI-ESM1-2-LR, see Fig. S3, S4). Overall, these simulated ther-
mocline ventilation pathways maintain a realistic meridional oxygen gradient with well oxygenated waters in the southern
basin and OMZ cores in the Arabian Sea and Bay of Bengal (contours of 20, 60 and 150 μmol/kg water extent shown in
solid black contours in Fig. 1 and Fig. S4). There are, however, ~~several regions of bias in the simulated oxygen field (Fig. 1g-i). For example,~~ significant biases in the oxygen field simulated in northern basin where the multi-model mean simulates
higher than observed oxygen levels in the ~~subsurface Arabian Sea~~ Arabian Sea, and lower than observed in the Bay of Bengal
(Fig. 1~~h). This is a well documented bias~~ g-i and Fig. S3). The high oxygen bias in the Arabian Sea is likely due to excessive
ventilation from marginal seas and southern source waters, though may also be influenced by deficiencies in parameterized
oxygen consumption rates and eddy-mixing rates (Schmidt et al., 2021), while the low oxygen bias in the Bay of Bengal is
possibly tied to the overestimation of oxygen consumption rates and remineralization depths (Al Azhar et al., 2017). These are
well documented biases among ESMs (Oschlies et al., 2008; Bopp et al., 2013; Rixen et al., 2020; Schmidt et al., 2021)~~that we~~
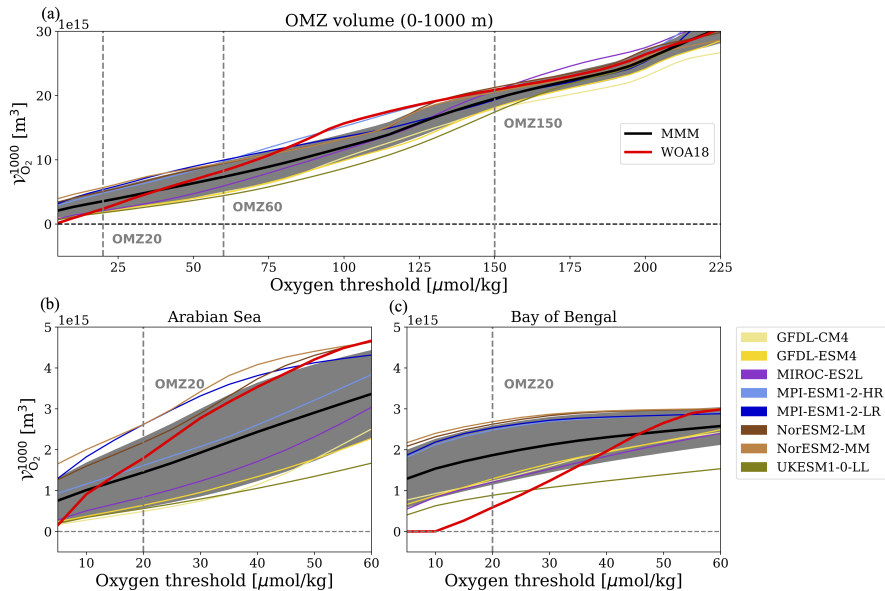
Figure 2. OMZ volume taken between 0-1000 m in the **(a)** Indian Ocean and sub-basins **(b)** Arabian Sea and **(c)** Bay of Bengal for the multi-model mean averaged over 1950-2015 (MMM; black) and observed climatology (WOA18; red). Shading represents one standard deviation of the model spread from the mean. Individual ESMs shown in colored curves.

significantly mitigated in . However, we have mitigated oxygen biases in the Arabian Sea in our ensemble by removing models
that lacked an OMZ core in the Arabian Sea lack suboxia there (Sect. 2.1; Fig. S5). S6).

Despite some biases in the multi-model mean oxygen field, we find good agreement with observed OMZ volumes. We compare thermocline OMZ volume ($\mathcal{V}_{O_2^{1000}}$, $\mathcal{V}_{O_2^{1000}}$ (i.e., volume in the upper 1000 m) , in observations and the multi-model mean for oxygen thresholds between 5 and 225 μmol/kg (Fig. 2a, $\mathcal{V}_{O_2^{1000}}$ for individual models are in Table S1.). In the observed climatology, $\mathcal{V}_{O_2^{1000}}$ increases about linearly with oxygen threshold, with an hypoxic volume OMZ60 ($<60\,\mu$mol/kg) of about
8.3×10^{15} m^3 and an OMZ150 volume a low oxygenated water volume OMZ150 ($<150\,\mu$mol/kg) of about 21×10^{15} m^3. The multi-model mean simulates this linear relationship and . In particular, it agrees with observations within 12% for % for the OMZ60 volume and within 7% for % for the OMZ150 volume, and at both benchmarks the observations fall within the ensemble spread . For the OMZ core ($<20\,\mu$mol/kg), with no clearly outlying ESM. The volume of the core OMZ20 is, however, overestimated by about 50% in the multi-model mean overestimates observed volumes by about 50% . The good agreement at hypoxic and higher thresholds arises from the realistic simulation of the southern Indian Ocean ventilation pathways that control these volumes. In contrast, the disagreement in the volume of the OMZ core primarily comes from the systematic overestimation of OMZ20 in the Bay of Bengal, a bias only partially offset by the underestimation of OMZ20 in the Arabian Sea (Fig. 2b,c).
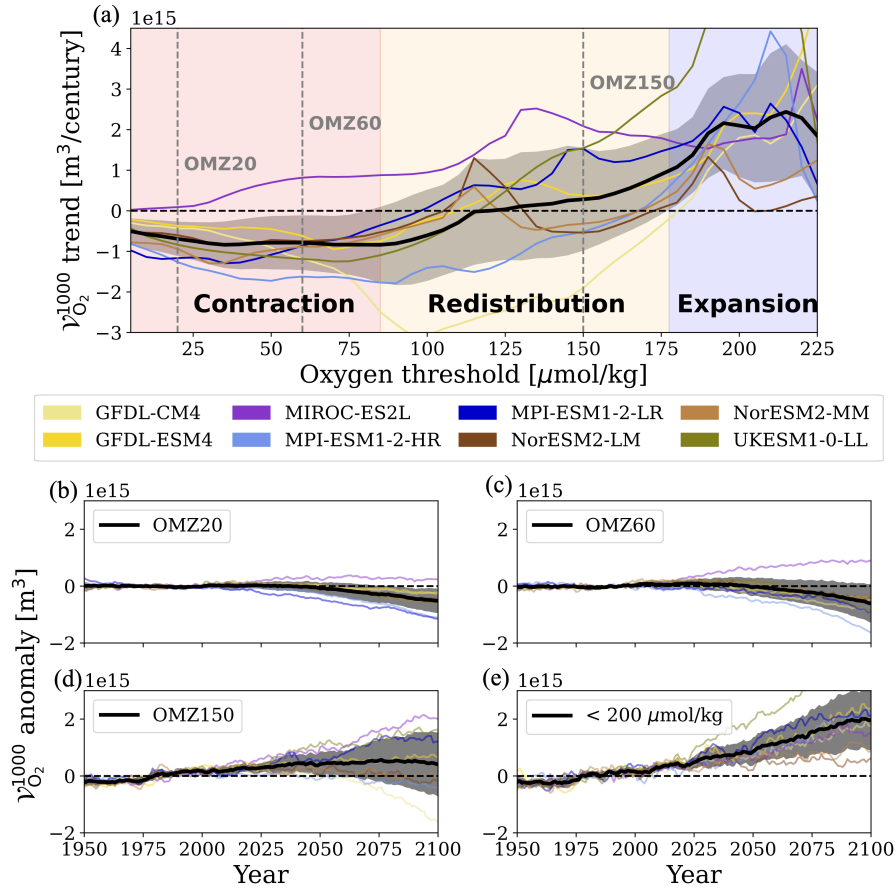
Figure 3. Multi-model mean thermocline OMZ volume changes (between 0 - 1000 m) under SSP5-8.5 scenario forcing (2015-2100). **(a)** $\mathcal{V}_{O_2^{1000}}$ trends as a function of oxygen threshold for the Indian Ocean. The 20, 60 and 150 μmol/kg thresholds bounding OMZ20, OMZ60 and OMZ150 are indicated with ~~dark blue and teal~~ gray dashed lines. **(b)** Time series of $\mathcal{V}_{O_2^{1000}}$ anomaly from 1950-2100 (anomaly referenced to 1950-2015 mean) for **(b)** OMZ20, **(c)** OMZ60 ~~(dark blue)~~ and **(d)** OMZ150~~(teal)~~, and **(e)** waters with $< 200\,\mu$mol/kg oxygen. Shading represents one standard deviation of model spread from the mean.

3.2 Projected OMZ volume exhibits diverging trends at low and high oxygen thresholds

290   Projections of thermocline OMZ volume under SSP5-8.5 forcing fall into three regimes: a robust expansion of ~~OMZ~~ volumes set by high oxygen thresholds (above $180\,\mu$mol/kg), a robust contraction of volumes set by low oxygen thresholds (below $85\,\mu$mol/kg), and a transition regime with weak and uncertain trends characterized by redistribution of ~~OMZ~~ volume (between 85 and $180\,\mu$mol/kg; Fig. 3a). We define robust OMZ expansion and contraction as where the multi-model mean trends exceed one standard deviation of the model spread. The ~~volume~~ volumes of hypoxic waters , (OMZ60~~, contracts

295   at a rate of~~) and core waters (OMZ20) contract at similar rates in the multi-model mean ($0.7\pm0.4\times10^{15}\,\mathrm{m}^3$/century and

0.8 ± 0.7~~$\times10^{15}\,\mathrm{m^3/century}$, with~~ $\times10^{15}\,\mathrm{m^3/century}$, respectively). The model spread is tighter for trends in OMZ20, and so the multi-model mean signal ~~emerging from the model spread only at the end of the twenty-first century~~ of volume trends emerges in the ensemble earlier for OMZ20 than for OMZ60 (Fig. 3~~b~~),c). About half of the OMZ20 contraction occurs in the Arabian Sea (Fig. S8). ~~This signal is similar for the OMZ core ($<20\,\mu\mathrm{mol/kg}$), where the multi-model mean projects a~~

~~contraction rate of $0.7\pm0.4\times10^{15}\,\mathrm{m^3/century}$.~~ Meanwhile, the volume of OMZ150 falls between the regimes of robust expansion and contraction and experiences near-zero volume ~~trends~~ changes in the multi-model mean ~~.~~ by 2100. Tracking the evolution of the OMZ150, we see that ESMs project an expansion over the historical period and first half of the twenty-first century before disagreeing on the trajectory in the latter half of the century~~(~~, with half of the ESMs projecting a contraction by 2100 (GFDL-CM4, MPI-ESM1-2-LR, UKESM1-0-LL, MIROC-ES2L) and the other half projecting an expansion (GFDL-CM4, MPI-ESM1-2-HR, NorESM2-LM, NorESM2-MM; Fig. 3~~b). By 2100, four ESMs project an expansion of the~~ d). Lastly, the volume of waters with less than $200\,\mu\mathrm{mol/kg}$ evolves similarly to the volume of the OMZ150 ~~and four project a contraction.~~ over the historical period, but then continues to follow a trajectory of robust expansion over the twenty-first century (Fig. 3e).

3.3 Regional contrasts in dissolved oxygen trends reshape the Indian Ocean OMZ

Projected trends in dissolved oxygen are highly variable in space, both horizontally and vertically, leading to regional contraction, expansion and redistribution of the OMZ volume (Fig. 4). The multi-model mean projects a weak increase in oxygen in the OMZ cores of the Arabian Sea and Bay of Bengal and a decline in oxygen in the relatively well oxygenated water masses entering via the Southern Pathway ~~and ventilating the OMZ outer layers~~ (Fig. 4). Strongest oxygen changes are, however, found at intermediate oxygen levels~~, between the core and the outer layers~~. We focus on the three major features that influence the OMZ volume at these intermediate levels (labeled by numbers in Fig. 4): the deoxygenation in the southeastern basin (Feature 1), the oxygenation of the western South Equatorial Current (Feature 2), and the deoxygenation in the northern Arabian Sea (Feature 3). ~~All three features of dissolved oxygen trends are captured in all individual ESMs in the ensemble (Fig. S6,S7), leading to a robust pattern in the multi-model mean (more than 75% of models agree on sign of trend; Fig. 4).~~ Feature 1 coincides with the flow of Southern Pathway Waters in the subtropical gyre and Indonesian Throughflow Water entering the Indian Ocean. Indeed, we see two distinct maxima of the deoxygenation along the meridional section at $90°$ E (Fig. 4c): one coinciding with Southern Pathway waters (namely Central, Mode and Intermediate Waters) centered around 500 m depth with deoxygenation rates up to $35\,\mu\mathrm{mol/kg/century}$, and one coinciding with Indonesian Throughflow waters at around 250 m depth with deoxygenation rates up to $50\,\mu\mathrm{mol/kg/century}$. Feature 2 is located where Southern Pathway Waters and Indonesian Throughflow waters mix within the South Equatorial Current. Feature 2 has a maximum oxygenation trend in the South Equatorial Current between 100 and 500 m, where waters oxygenate at a rate of up to about $50\,\mu\mathrm{mol/kg/century}$, and a secondary maximum in the North Equatorial Current, with oxygenation rates up to $40\,\mu\mathrm{mol/kg/century}$ (Fig. 4a-b). Together, Features 1 and 2 form an ~~oxygenation~~ oxygenation-deoxygenation dipole along the path of the South Equatorial Current. Lastly, Feature 3 is a deoxygenation at a rate of up to about $60\,\mu\mathrm{mol/kg/century}$ in the northern Arabian Sea between about 100 and 300 m depth, a region where the Persian Gulf Outflow ~~dominates~~ (observed down to about 400 m depth) and winter convection (observed mixed layers down to about 100 m depth) dominate ventilation (Fig. 4a-b). ~~Waters in Feature~~
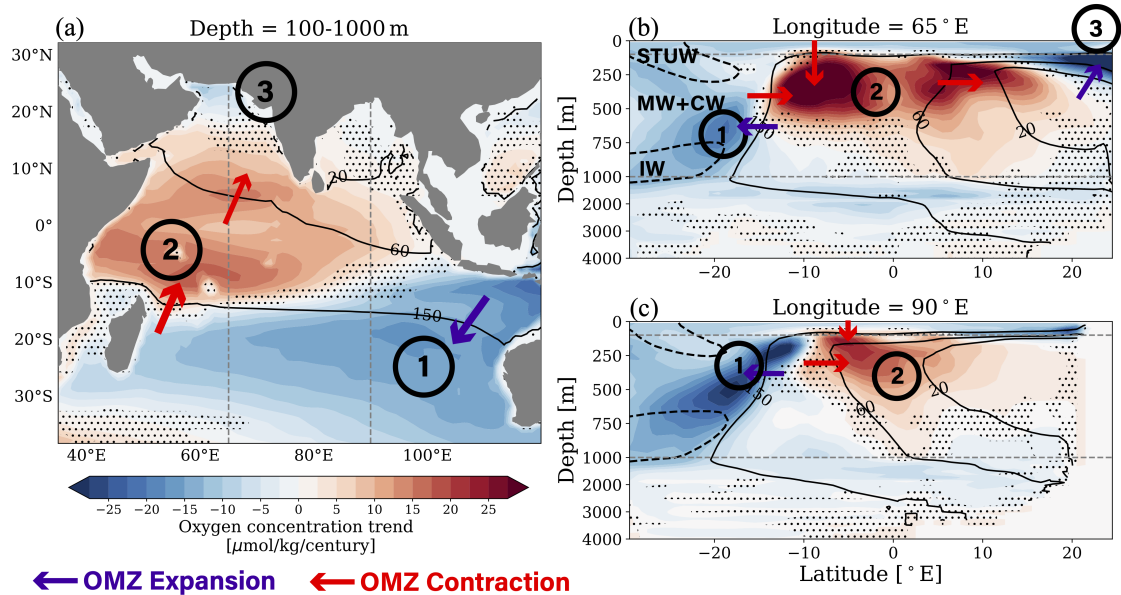
Figure 4. Multi-model mean (MMM) dissolved oxygen trends under SSP5-8.5 scenario forcing (~~1915-2100~~2015-2100). Dissolved oxygen trends **(a)** bewtween 100 and 1000 m, **(b)** at 65°E and **(c)** at 90°E. Dashed gray lines mark **(a)** 65°E and 90°E, and **(b,c)** 100 and 1000 m. ~~(b,c)~~ Solid black contours represent 20, 60 and 150 μmol/kg oxygen. Dashed black contours highlight salinity signatures of Subtropical Underwater (STUW) and Intermediate Water (IW), with Central Water (CW) and Mode Water (MW) between. Main features of dissolved oxygen trends numbered, with effect on OMZ volume indicated by purple and red arrows. Results are stippled where less than 75 % (6/8) of models agree on sign of trend.

330   The three features of dissolved oxygen trends are simulated by all individual ESMs in the ensemble (Fig. S9,S10), leading to a robust pattern in the multi-model mean (more than 75 % of models agree on sign of trend; Fig. 4). However, there are some notable differences in their amplitude and extent across the ensemble. Here, we leverage comparisons between models that share the same architecture, but differ either in their horizontal resolution or the complexity of their biogeochemical module, to illustrate the sensitivity of the oxygen response to the model characteristics. For example, GFDL-CM4 and GFDL-ESM4 have
335   the same dynamical ocean model but differ in both oceanic and atmospheric resolution (GFDL-CM4 has higher resolution) and biogeochemical components (GFDL-ESM4 has more complex representation of biogeochemistry) (Dunne et al., 2020; Held et al., 2019) . Despite very similar historical representations of oxygen in the Indian Ocean, GFDL-CM4 and GFDL-ESM4 simulate different strengths of oxygenation in the SEC (Feature 2) and deoxygenation in the Arabian Sea (Feature 3~~deoxygenate at a rate of up to about 60 μmol/kg/century.~~), with GFDL-CM4 projecting more pronounced features in both regions (Fig. S10).
340   Meanwhile, NorESM2-LM and NorESM2-MM, which differ only in the horizontal resolution of their atmospheric components (Seland et al., 2020), project similar trends for oxygenation in the SEC but differ on the strength of the deoxygenation in the Arabian Sea, with weaker deoxygenation simulated in the higher atmospheric resolution version (NorESM2-MM; Fig. S10). Finally, CanESM5 and CanESM5-CanOE only differ in the complexity of their biogeochemical model (Christian et al., 2022)

14

. Both CanESM models were removed from our multi-model mean due to the absence of suboxia in the Arabian Sea, but we use them here to illustrate the sensitivity to the biogeochemical complexity. CanESM5-CanOE, which has a more complex representation of biogeochemistry, projects weaker oxygenation in the SEC and stronger deoxygenation in the Arabian Sea than the simpler CanESM5 model. These results suggest that the sign of oxygen change is robust across the ensemble, but that both model resolution (atmospheric and oceanic) and biogeochemical complexity influence the amplitude of the change.

These three features ultimately explain the contraction, expansion, and redistribution of the OMZ volume at thermocline depths across oxygen thresholds. The deoxygenation of ~~in~~ the southeastern basin (Feature 1) is the primary driver of ~~OMZ~~ the volume expansion at high oxygen thresholds (~~expansion regime~~ $> 180\,\mu$mol/kg, Fig. 3b). The ~~oxygenation~~ oxygenation-deoxygenation dipole (from Features 1 and 2) ~~redistribute~~ redistributes the OMZ volume from west to east and explains the weak volume changes found at intermediate oxygen thresholds (between 85 and 180 μmol/kg) including the volume of the OMZ150 (redistribution regime, Fig. 3b). The oxygenation in the South Equatorial Current, and in turn the western boundary current waters (Feature 2), contributes to the OMZ contraction at low oxygen thresholds including the volume of OMZ60 (contraction regime, Fig. 3b), although the net change in volume is relatively small due to the compensating expansion in the northern Arabian Sea which also affects the low oxygen thresholds (Feature 3).

### 3.4 Dissolved oxygen trends are dominated by changes in ventilation

To identify which processes control projected dissolved oxygen trends, and in turn the reshaping of the Indian Ocean OMZ, we separate dissolved oxygen trends into thermal and non-thermal components (Fig. 5). Thermal oxygen trends relate to changes in oxygen saturation concentrations, while non-thermal oxygen trends arise from changes in physical ocean circulation and biological respiration rates (Sect. 2.2.2). Thermal and non-thermal effects tend to influence different water masses: thermal trends are strongest in surface waters (above 100 m), while non-thermal trends are strongest at thermocline depths (100 to 1000 m), but are also responsible for deoxygenation in the deep ocean (below 1000 m) (Fig. 5). Thermal oxygen changes drive relatively uniform deoxygenation in the surface ocean of about 5 to 15 μmol/kg/century. Thermal effects are only significant below 100 m along the pathways of Subtropical Underwater (Fig. 5b) and Indonesian Throughflow Water (Fig. 5a,c). The non-thermal component largely explains the strong patterns of oxygenation and deoxygenation discussed above, including deoxygenation in the southeast, oxygenation in the SEC, and deoxygenation in the northern Arabian Sea (Features 1 to 3; Fig. 4 and 5d-f).

The ideal age of seawater, or the average time since water has been exposed to the surface, is a direct measure of ventilation timescale; trends in ideal age thus indicate changes in the rate of ventilation from advection and mixing. Trends in ideal age agree with the pattern of non-thermal oxygen trends. The regions of maximum decreased ventilation (i.e., waters get older) correspond spatially with deoxygenation in the southeastern basin (Feature 1) and Arabian Sea (Feature 3), while the region of maximum increased ventilation (i.e., waters get younger) corresponds to the region of oxygenation in the South Equatorial Current (Feature 2; Fig. ~~??). We further quantify the tight link between changes in ventilation and the non-thermal oxygen trends controlling oxygenation/deoxygenation patterns by computing the Pearson Correlation Coefficients between interannual anomalies in ideal age and non-thermal oxygen. Deviations from a correlation coefficient of unity can arise either~~
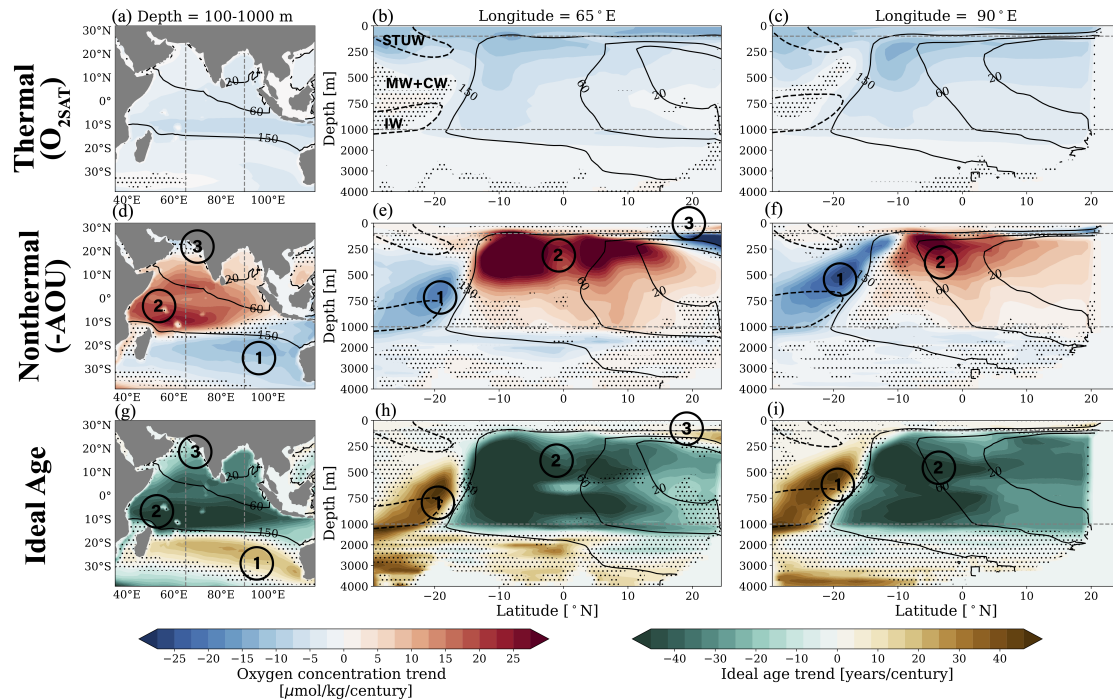
Figure 5. Thermal and non-thermal components of multi-model mean (MMM) dissolved oxygen trends under SSP5-8.5 scenario forcing (~~1915-2100~~2015-2100). Thermal oxygen (O_{2SAT}) trends **(a)** between 100 and 1000 m, **(b)** at 65°E and **(c)** at 90°E. Non-thermal oxygen (-AOU) trends **(d)** between 100 and 1000 m, **(e)** at 65°E and **(f)** at 90°E. Multi-model mean (MMM) ideal age trends **(g)** between 100 and 1000 m, **(h)** at 65°E and **(i)** at 90°E. Dashed gray lines mark **(a,d)** 65°E and 90°E, and ~~(b,c,e,f)~~ **(b,c,e,f,h,i)** 100 and 1000 m. ~~(b,c,e,f)~~ Solid black contours represent 20, 60 and 150 μmol/kg oxygen. Dashed black contours represent salinity contours highlighting Subtropical Underwater (STUW) and Intermediate Water (IW), with Central Water (CW) and Mode Water (MW) between. Main features of dissolved oxygen trends numbered. Results are stippled where less than 75 % (6/8) of models agree on sign of trend.

380   ~~from changing biological oxygen demand or from the mixing of many source water masses (see Appendix **??** for details), while a coefficient of unity represents the special case where non-thermal oxygen trends are controlled by ventilation changes along a single pathway. Ventilation and non-thermal oxygen changes are well correlated (0.8-1.0)along the northern edge of the South Indian Gyre associated with Southern Pathway Waters (Feature 1), in the region of oxygenation in the South Equatorial Current (Feature 2) and in the northern Arabian Sea (Feature 3). Thus, there is strong evidence~~ 5ghi, Fig. S11). This suggests that changes in physical ventilation pathways are the main control of features of dissolved oxygen change, and ultimately the reshaping of OMZ volume, in the Indian Ocean.

16
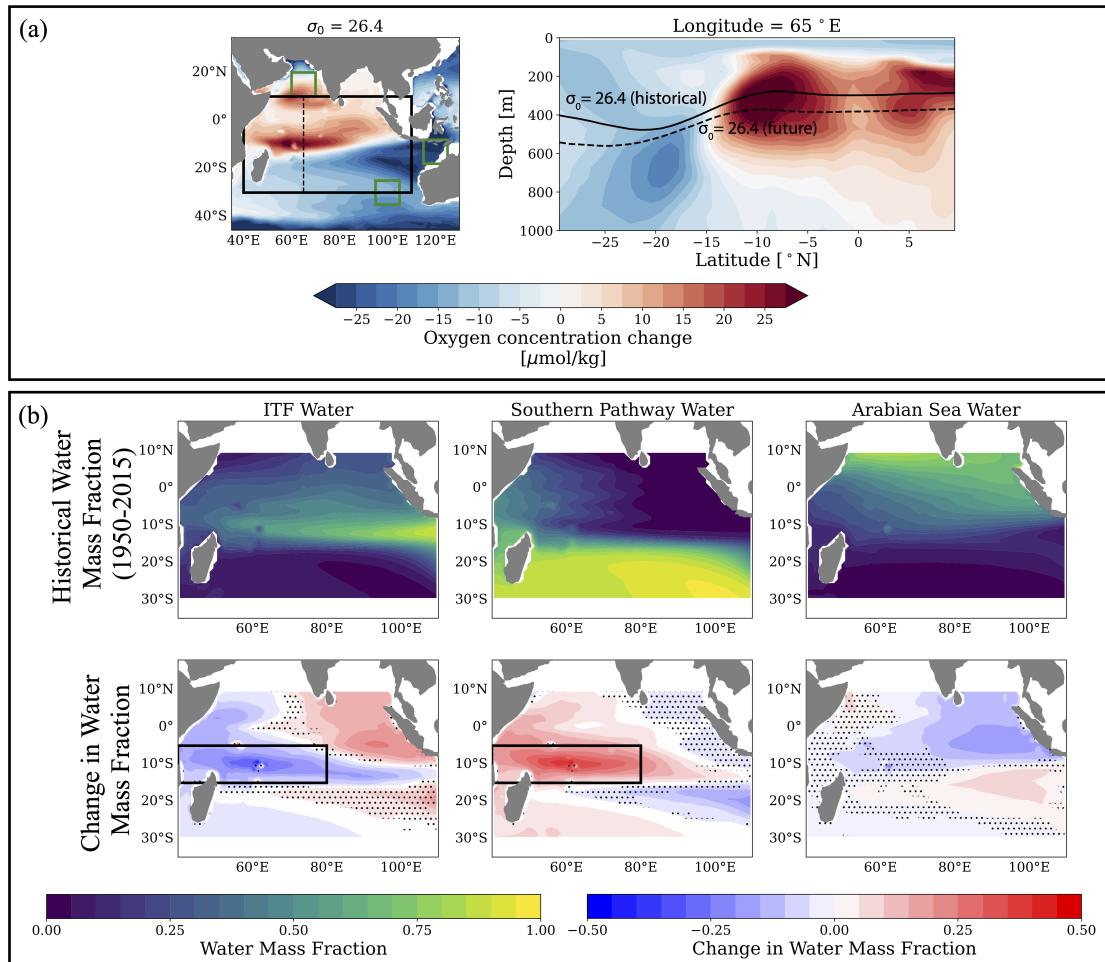
Figure 6. Multi-model mean (MMM) results of Optimum Multiparameter (OMP) ~~mixing model~~ analysis in the South Equatorial Current (SEC). **(a)** Oxygen changes along the $\sigma_0 = 26.4$ surface and the historical (solid) and end-of-century (dashed) depth of $\sigma_0 = 26.4$ indicated over MMM oxygen changes in depth space at $65\,°E$. Green boxes mark source water regions and solid black box represents region for which water mass fractions are solved. (b) Historical distribution of Indonesian Throughflow, Southern Pathway, and Arabian Sea Water fractions, and changes in water mass fractions between historical and end-of-century states. Historical states calculated as 1950-2015 mean, and end-of-century states calculated as historical mean plus linear trends over 2015-2100. Solid black boxes in (b) show region of western SEC. Stippling where less than 75 % (6/8) of models agree on sign of change.

3.5 Shifts in water mass ~~mixing~~ composition control oxygenation in South Equatorial Current

In this and the following section, we attribute the significant features of projected oxygen trends in the Indian Ocean thermocline to specific changes in ventilation pathways. Perhaps the most remarkable aspect of projected dissolved oxygen changes in

the Indian Ocean under SSP5-8.5 forcing is the ~~oxygenation~~ oxygenation-deoxygenation dipole along the ~~SEC~~South Equatorial Current (SEC) (Features 1 and 2). The two major ventilation pathways in this region are the Southern Pathway Waters and Indonesian Throughflow Water. The transport of these two pathways is projected to decline between 100 and 1000 m over the twenty-first century (Fig. ~~??a~~S12). The transport of Southern Pathway ~~Waters~~Water across 30°S is projected to decline by 4.4±3.2 Sv/century (from 53±2 Sv) and the transport of Indonesian Throughflow ~~Waters~~Water by 5.1±2.0 Sv/century ~~(Fig. ??a~~from (15±3 Sv). The weakening of these transport pathways can ~~easily~~ explain the deoxygenation in the southeastern Indian Ocean where each pathway acts as a single dominant source (thus accounting for Feature 1). Curiously, however, this weakened transport seems in apparent contradiction with the increased ventilation and oxygenation of the western ~~South Equatorial Current~~ SEC (Fig. 4). We hypothesize that this oxygenation must arise from a shift in the ~~mixing ratio~~ relative contributions between these source waters in the western ~~South Equatorial Current~~ SEC where they co-dominate, favoring relatively young and oxygen-rich waters from the Southern Pathway over relatively old and oxygen-poor waters from the Indonesian Throughflow. To ~~motivate this hypothesis, we show a time series of the ratio of inflowing volume transport from Southern Pathway Waters and Indonesian Throughflow Water at between 100 and 1000 m (Fig. ??b), demonstrating that this ratio increasingly favors Southern Pathway Waters over the twenty-first century. To~~ test this hypothesis, we ~~solve a mixing model~~ perform an OMP analysis (Tomczak and Large, 1989) in the tropical Indian Ocean for both a historical mean state (1950-2015) and an end-of-twenty-first-century mean state (climatological 2100) at a potential density layer within the thermocline, nominally $\sigma_0 = 26.4$ (Sect. 2.2.4). This potential density layer intersects the dipole of oxygen change (Features 1 and 2) in the South Equatorial Current (Fig. 6a). We solve for the ~~mixing~~ fractions of three source waters: Indonesian Throughflow Water, Southern Pathway ~~Waters~~Water and Arabian Sea Water (oxygen minimum water~~) (~~; Sect. 2.2.4). ~~The mixing model identifies a reasonable historical water mass distribution with Indonesian Throughflow Waters~~ We find that the OMP analysis is able to reconstruct historical and future oxygen, temperature and salinity in this region with composites of source water types (see Fig. S13 for a comparison of simulated and reconstructed states in the Feature 2 region).

In the multi-model mean historical state, the OMP analysis highlights Indonesian Throughflow Water originating from the main straits of the Indonesian Throughflow and penetrating across the basin along 10°S, and Southern Pathway ~~Waters~~Water residing primarily within the southern gyre until ~~they join~~ it joins the western boundary current (Fig. 6b; in agreement with observed distribution from Tomczak and Large, 1989). Specifically, the OMP suggests that waters in the region of Feature 2 in the western SEC are composed of about 40 % Indonesian Throughflow Water, 30 % Southern Pathway Water and 30 % Arabian Sea Water in the multi-model mean (average composition between 40-80°E and 5-15°S, Fig. 6b). Under SSP5-8.5 forcing, there is a significant shift in ~~mixing ratios~~ water mass fractions in the western ~~South Equatorial Current~~ SEC away from Indonesian Throughflow ~~Waters~~Water in favor of Southern Pathway ~~Waters~~Water between the historical and future states. ~~For instance, at 65°E and 10°S, Indonesian Throughflow Waters historically accounts for over 50% of the local water mass while~~ By the end of the century, the composition of this region is projected to shift to about 20 % Indonesian Throughflow water and 55 % Southern Pathway Water (changes of -.2 and +.25 water mass fractions for Indonesian Throughflow and Southern Pathway Waters~~accounts for about 10%. This shifts to nearly 50% Southern Pathway Waters and less than 30% Indonesian Throughflow Waters in the future state. Using nominal historical oxygen concentrations of each source water— 230, 135, and~~

~~40 μmol/kg for Southern Pathway, Indonesian Throughflow , and~~, respectively), while the contribution of Arabian Sea Water stays relatively constant (Fig. 6b).

In all ESMs except one (MPI-ESM1-2-LR), the simulated oxygenation in the western SEC is well approximated by the change in oxygen supply associated with the shift in source water composition in the OMP (simulated ΔO_2 and oxygen supply reconstructed from water mass compositions, $\Delta O_{2,supply}$, fall within $\pm 5\,\mu$mol/kg of the 1-to-1 line in Fig. 7a). This suggests that changes in remineralization of oxygen might have a relatively low influence compared to changes in transport (Sect. 2.2.4). Furthermore, nearly all of the changes in oxygen can be accounted for by the changing supply from the Indonesian Throughflow and Southern Pathway (ΔO_2 and $\Delta O_{2,supply}$ from ITF and SPW alone fall near the 1-to-1 line in 7b). That is, the oxygenation in the western SEC can be accounted for by a shift away from oxygen-poor Indonesian Throughflow Water in favor of oxygen-rich Southern Pathway Water. We note that MPI-ESM1-2-LR is the only ESM in the ensemble which behaves qualitatively differently than the multi-model mean, projecting an increased influence of Indonesian Throughflow Water, and weakened influences of Southern Pathway and Arabian Sea Waters ~~, respectively— this shift in composition can account for about a 50 μmol/kg increase in oxygen. This new~~ in this region (not shown). MPI-ESM1-2-LR is also the only model that requires significant contributions from remineralization to explain the simulated changes in oxygen. Specifically, the OMP requires significantly weaker remineralization in the future state than in the historical state to match the simulated oxygen fields (larger oxygenation ΔO_2 than reconstructed from OMP $\Delta O_{2,supply}$ for MPI-ESM1-2-LR in Fig. 7a).

The modified water mass composition in the western SEC is then propagated across the equator by the western boundary current along the Somali coast and then ~~East~~ east into the basin interior by the North Equatorial Current, increasing ventilation in the northern basin and accounting for the secondary oxygenation maximum north of the equator (Fig. 6b). A previous study found that ESMs projected a strengthening of the cross-equatorial transport and North Equatorial Current with warming (Sharma et al., 2023), which may in turn strengthen the northern oxygenation maximum. We note that despite the movement of the $\sigma_0 = 26.4$ surface between the historical and end-of-century states, the results here are not an artifact of this isopycnal displacement (Fig~~S8~~. S14)

3.6 Shoaling marginal sea outflows shift ventilation in the Arabian Sea

We perform a similar analysis as above to ~~attribute the~~ assess the role of changing ventilation pathways, namely marginal sea outflows, to the deoxygenation projected in the northern Arabian Sea (Feature 3)~~to changes in ventilation pathways, namely from marginal sea outflows~~. Unlike pathways in the southern Indian Ocean, the overall strength of marginal sea outflow ~~transports~~ transport remains steady under SSP5-8.5 forcing (Fig. ~~??~~S12). Neither the Persian Gulf outflow nor the Red Sea outflow show any robust trends in volume transport across the ESM ensemble. We hypothesize that, although overall transport from marginal seas does not change, the buoyancy of outflow plumes increases with the rapid heating of marginal seas, which can shoal the outflow plumes and reduce ventilation of the OMZ at thermocline depths. This hypothesis is motivated by the findings of Lachkar et al. (2019), who find that this mechanism can have a strong influence on the OMZ in the Arabian Sea. To test this, we ~~solve a mixing model~~ perform an OMP analysis along the nominal potential density layer $\sigma_0 = 25.7$, which corresponds to the region of deoxygenation in the Arabian Sea (Feature 3; Fig. 8a). We define three source waters for the

## Western South Equatorial Current (Feature 2)
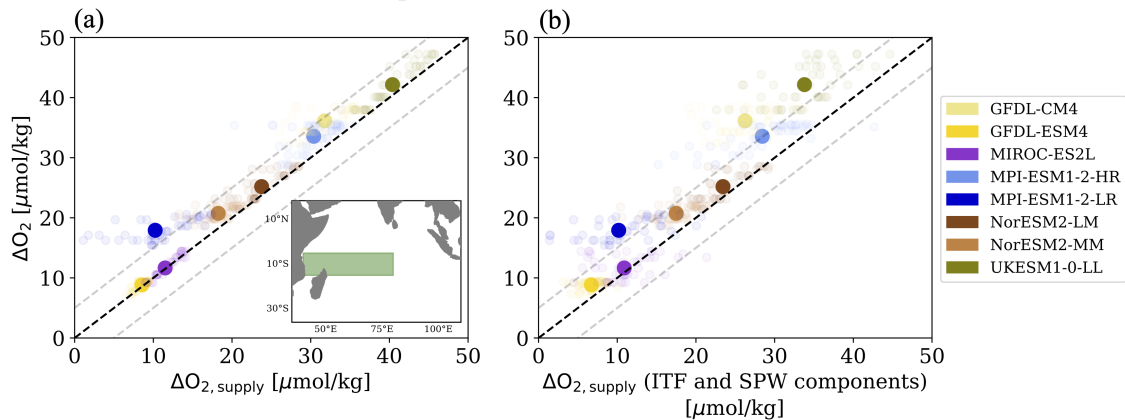
Figure 7. ~~Interannual transport anomalies (referenced to 1950-2015 mean) of marginal sea outflows~~ Dissolved oxygen changes computed from ~~Persian Gulf~~ water mass composition changes, $\Delta O_{2,supply}$, versus total simulated dissolved oxygen changes in the western South Equatorial Current (~~blue~~indicated by inset in panel **(a)**). **(a)** $\Delta O_{2,supply}$ from all source water changes. **(b)** $\Delta O_{2,supply}$ only from contributions of Indonesian Throughflow and ~~Red Sea (orange)~~Southern Pathway Waters. Solid ~~curves represent multi-model~~ markers are mean of all samples (~~MMM~~faded markers)~~and shading represents one standard deviation of model spread.Transport data is available for 5 ESMs.~~

region: Persian Gulf Water, Red Sea Outflow Water and Arabian Sea Water (Sect. 2.2.4). ~~In the~~ We find that the OMP analysis is able to reconstruct historical and future oxygen, potential temperature and salinity from the three source water types in the northern Arabian Sea region (see Fig. S15 for a comparison of simulated and reconstructed states in the region of Feature 3).

460   In the multi-model mean historical state (1950-2015), Persian Gulf Water spreads from the Gulf of Oman across the northern Arabian Sea and Red Sea Water spreads from the Gulf of Aden, while Arabian Sea Water acts as the ambient water in the basin (Fig. 8b). In the region of Feature 3 (between 60-70°E and 20-25°N), Persian Gulf Water accounts for about 65 % of the water mass in the multi-model mean historical state. Concurrent with the region of deoxygenation in the northern Arabian Sea, there is a ~~pronounced~~ decrease in the presence of Persian Gulf Water in the end-of-century mean, which gets replaced

465 by ambient Arabian Sea Water. ~~In the historical state,~~ Averaged over the region of Feature 3, the contribution of Persian Gulf Water ~~accounts for about 60% of the water mass at 65°E, 23°N, but this contribution is reduced to approximately 30% in the end-of-century state. This decrease in ventilation from the~~ decreases to 55 % by the end of the century (decrease in water mass fraction of about .1; Fig. 8b). This is also associated with a shift in Persian Gulf Water ~~can explain the deoxygenation simulated between 100 and 300 m. The mixing model also suggests~~ westward. Further south, there is a decrease in ventilation from Red

470 Sea Outflow Water along $\sigma_0 = 25.7$, which may contribute ~~weakly~~ to deoxygenation off of the Omani coast (Fig. 8b). ~~We note that~~

    In five out of the seven ESMs, the simulated deoxygenation in the northern Arabian Sea is well approximated by the change in oxygen supply reconstructed from the shift in water masses in the OMP (ΔO_2 and $\Delta O_{2,supply}$ fall within $\pm 5\,\mu mol/kg$ of
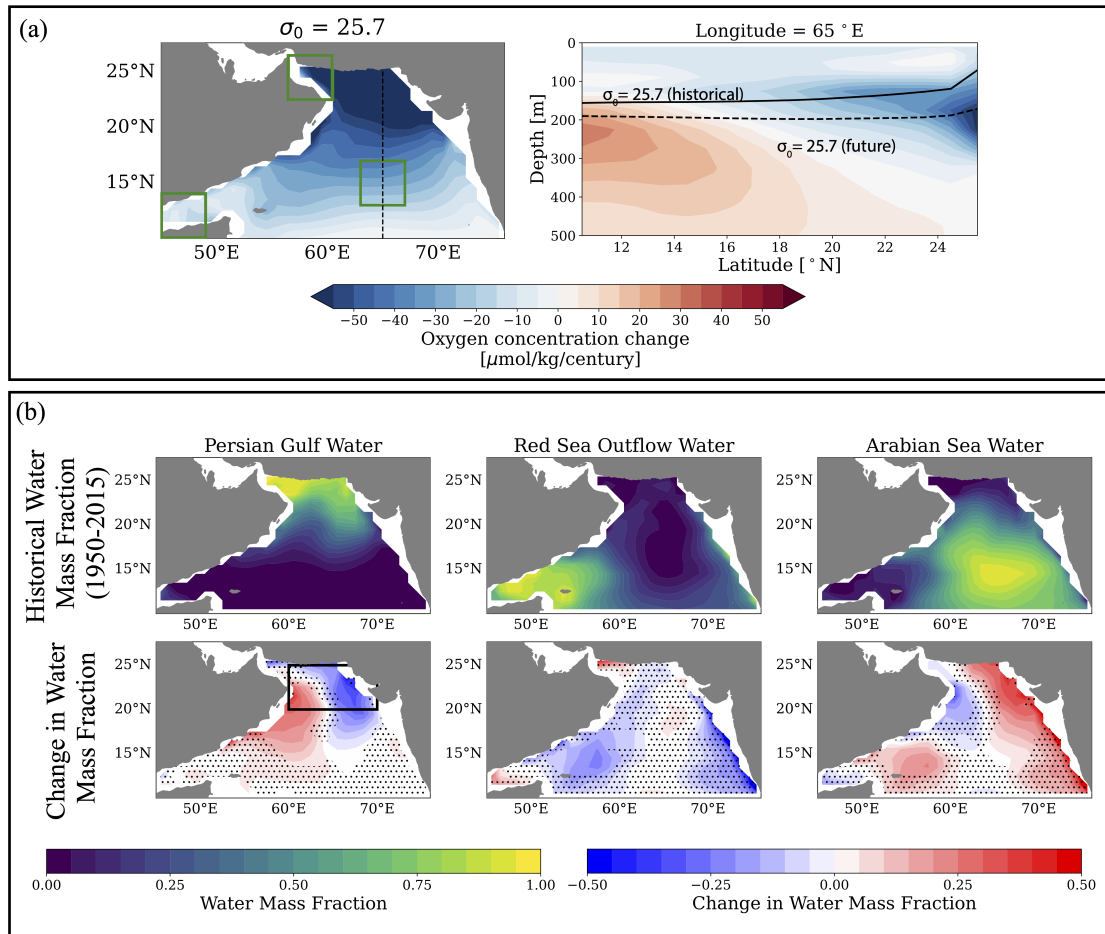
Figure 8. Multi-model mean (MMM) results of Optimum Multiparameter (OMP) ~~mixing model~~ analysis in the Arabian Sea. **(a)** Oxygen changes along the $\sigma_0 = 25.7$ surface and the historical (solid) and end-of-century (dashed) depth of $\sigma_0 = 25.7$ indicated over MMM oxygen changes in depth space at $65\,°E$. Green boxes mark source water regions. **(b)** Historical distribution of Persian Gulf, Red Sea Outflow, and Arabian Sea Water fractions, and changes in water mass fractions between historical and end-of-century states. Historical states calculated as 1950-2015 mean, and end-of-century states calculated as historical mean plus linear trends over 2015-2100. Solid black box in (b) show region of northern Arabian Sea over which we report changes. Stippling where less than 75 % (6/8) of models agree on sign of change

the 1-to-1 line in Fig. 9a). We find that the majority of this deoxygenation in the region can be accounted for by changes in oxygen supply by the Persian Gulf (ΔO_2 and $\Delta O_{2,\text{supply}}$ from Persian Gulf Water alone fall close to the 1-to-1 line in Fig. 9b). We note that two ESMs (MPI-ESM1-2-HR and MPI-ESM1-2-LR) exhibit weaker $\Delta O_{2,\text{supply}}$ than ΔO_2 (ESMs fall below the 1-to-1 line in Fig. 9a). While this may suggest that remineralization increases between the historical and future states in these

Northern Arabian Sea (Feature 3)
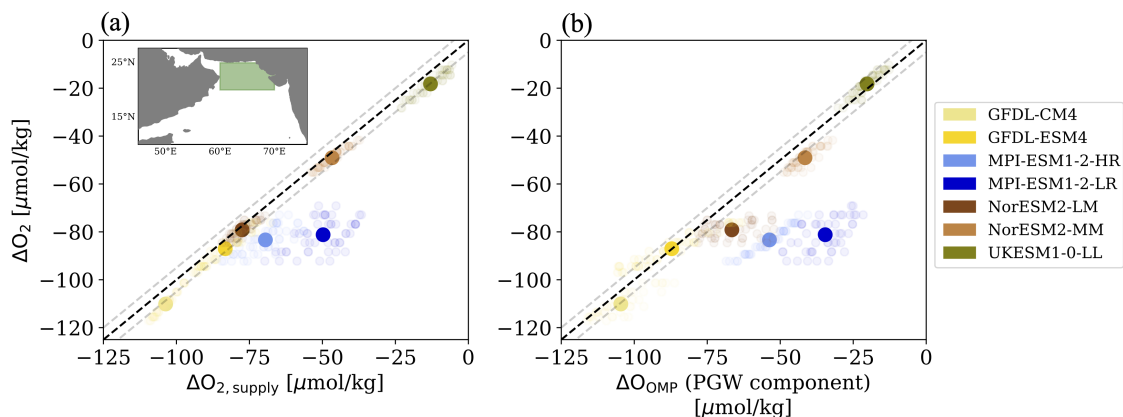
Figure 9. Dissolved oxygen changes computed from water mass composition changes, $\Delta O_{2,\text{supply}}$, versus total simulated dissolved oxygen changes in the northern Arabian Sea (indicated by inset in panel **(a)**). **(a)** $\Delta O_{2,\text{supply}}$ from all source water changes. **(b)** $\Delta O_{2,\text{supply}}$ only from contributions of Indonesian Throughflow and Southern Pathway Waters. Solid markers are mean of all samples (faded markers).

ESMs, this is unlikely given projected changes in export of organic carbon (see next section). Rather, it is likely that the region is poorly described by the source water types given to the OMP in these two ESMs.

480   We note that for an alternative analysis where the future state is evaluated at a potential density layer which aligns approximately with the historical depth of $\sigma_0 = 25.7$ (i.e., ~~any~~ aliasing from isopycnal displacement is removed; Sect. 2.2.4; Fig. ~~S9~~S16), we see ~~even~~ greater agreement between the pattern of deoxygenation and decreases in Persian Gulf Water fraction.

4 ~~Discussion and Conclusions~~

3.1 Contributions of biological and stratification changes to oxygen changes

485 ~~We examine the changes in~~

    The OMP analysis suggests that nearly all of the simulated oxygen changes in the western SEC and northern Arabian Sea can be accounted for by shifts in water mass compositions driven by changes in advective ventilation pathways (Fig. 7, 9). However, the residual oxygen changes that the OMP analysis does not capture, while small for most ESMs, tend to be systematically biased positive for the western SEC and negative for the northern Arabian Sea. This suggests the influence of 490 additional processes not accounted for in the reconstruction of oxygen supply from the OMP analysis, in particular the increase in subsurface stratification expected with global warming that can influence the vertical mixing between different water masses, and changes in biological oxygen consumption along advective pathways once a water parcel has left its source water region.

    We examine trends in stratification (for the eight ESMs) and the export of organic carbon at 100 m (available for seven out of eight ESMs) under SSP5-8.5 forcing. Strongest stratification increases are generally confined to the upper 100 m of
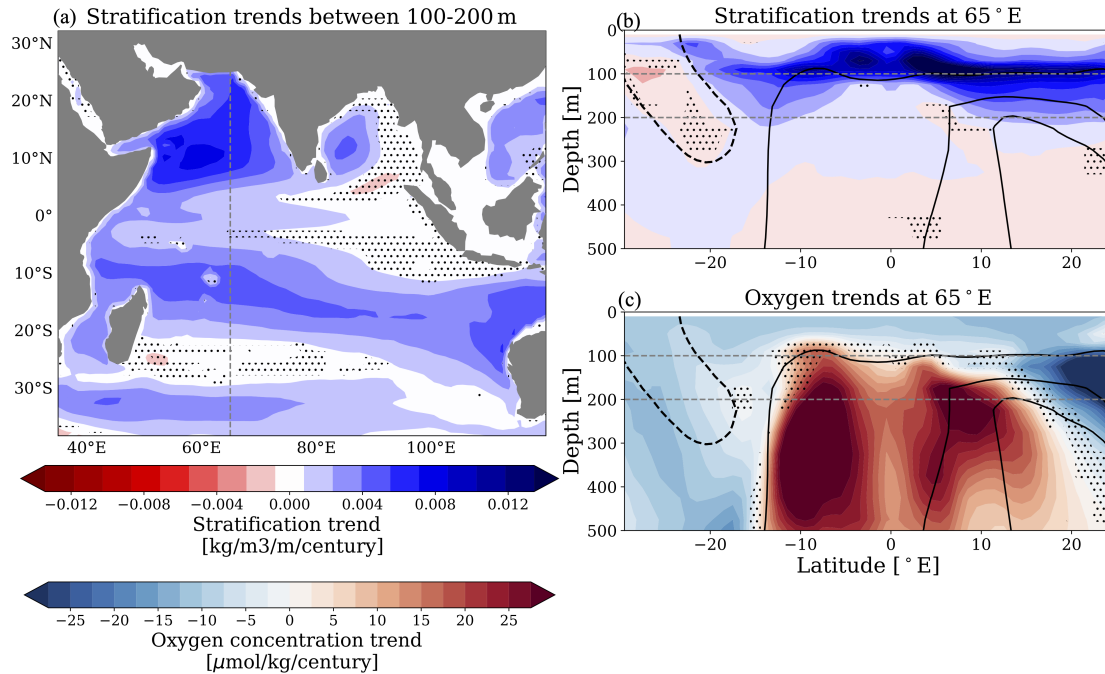
Figure 10. Multi-model mean (MMM) stratification trends under SSP5-8.5 scenario forcing (2015-2100). Stratification trends **(a)** between 100 and 200 m and **(b)** at 65°E. **(c)** Dissolved oxygen trends at 65°E. Dashed gray lines mark **(a)** 65°E and 90°E, and **(b,c)** 100 and 200 m. Solid black contours represent 20, 60 and 150 μmol/kg oxygen. Dashed black contours highlight salinity signatures of Subtropical Underwater (STUW). Results are stippled where less than 75 % (6/8) of models agree on sign of trend.

the water column, but in both the Arabian Sea and SEC regions, the multi-model mean simulates significant stratification increases between 100 and 200 m (about 0.005 $\mathrm{kg/m^3}$/m/century, Fig. 10). These stratification increases are simulated consistently across the ESM ensemble for both regions (Fig. S17). The oxygenation in the SEC region occurs mostly below 200 m, where stratification does not show strong changes, suggesting that changes in vertical mixing likely play a relatively minor role in this region (Fig. 10b,c). In contrast, the deoxygenation in the northern Arabian Sea is largely collocated with the increase in stratification simulated between 100 and 200 m, suggesting that reduced vertical mixing of oxygenated surface waters downward contributes to the deoxygenation projected in this region. Increased subsurface stratification tends to limit the vertical mixing of oxygenated surface waters downward, but also limits the mixing of subsurface nutrients into the surface, which in turn limits primary productivity, the export of organic matter at depth, and potentially reduces the consumption of oxygen in the subsurface. The export of organic carbon consistently declines under SSP5-8.5 forcing over the Indian Ocean in the multi-model mean, with local maximum declines in the western SEC, the Bay of Bengal and the Arabian Sea (Fig. 11 and Fig. S18 for individual ESMs), suggesting a decline in the consumption of oxygen along ventilation pathways.
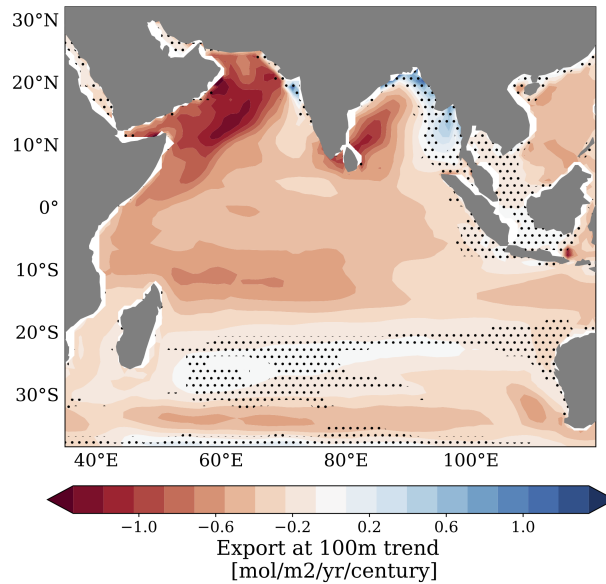
Figure 11. Multi-model mean (MMM) export of organic carbon at 100 m trends under SSP5-8.5 scenario forcing (2015-2100). Results are stippled where less than 75 % (6/8) of models agree on sign of trend.

The projected decline in export and increase in stratification have opposing effects on oxygen changes, and are therefore at least partially offsetting each other. The CMIP6 archive does not provide the necessary data to quantify the contributions of these two factors on oxygen changes. However, the signs of the residual oxygen changes that remain unexplained by the OMP analysis can provide some qualitative information on the relative contributions of these two processes. Positive residuals (i.e. stronger oxygenation simulated in ESMs than reconstructed by the OMP analysis; Fig. 7) suggests that the decline in export dominates over the increase in stratification in the western SEC. In contrast, negative residuals (i.e., stronger deoxygenation simulated in ESMs than reconstructed by the OMP analysis, Fig. 9) suggest that the influence of increased stratification exceeds the influence of reduced export in the northern Arabian Sea.

4   Discussion

We examine the changes in dissolved oxygen and OMZ volume in response to the high-emissions scenario forcing (SSP5-8.5scenario) in the Indian Ocean using an ensemble of eight CMIP6-generation CMIP6 Earth system models. In the following, we discuss the three regimes that characterize the OMZ response to warming in the Indian Ocean thermocline (upper 1000 m). We compare this response to that previously investigated for the Pacific Ocean OMZ and to the unstudied response for the Atlantic OMZ, and contrast the OMZ changes projected in the thermocline to the changes projected in the deep ocean (Fig. 12). We also revise the existing "single-pipe" and "mixing-network" ventilation framework to interpret the OMZ response

of the Indian Ocean, discuss observational constraints on ventilation pathways, and consider caveats in the model ensemble projections.

4.1 Three-regime response of the oxygen minimum zone

525 The response of oxygen and the OMZ in the Indian Ocean thermocline (upper 1000 m) falls into three regimes (Fig. 3a and 12a): a contraction of ~~the OMZ~~ volume delimited by low oxygen thresholds ($<85\,\mu\mathrm{mol/kg}$), an expansion of ~~the OMZ~~ volume delimited by high oxygen thresholds ($>180\,\mu\mathrm{mol/kg}$), and a redistribution of the ~~OMZ volume with relatively weak volume changes~~ volume at intermediate oxygen thresholds (85 to $180\,\mu\mathrm{mol/kg}$). This three-regime response is similar to the OMZ response described in the Pacific Ocean by Busecke et al. (2022) (Fig. 12b). A striking difference between the two basins,

530 however, is the widespread oxygen gain projected in the Indian Ocean. Indeed, ESMs robustly project an oxygenation of the OMZ cores in the Arabian Sea and Bay of Bengal, similar to the Pacific OMZ core, but also an oxygenation of the southwest Indian Ocean along the path of the South Equatorial Current and North Equatorial Current. As a result, the OMZ contracts for thresholds as high as $85\,\mu\mathrm{mol/kg}$ (including the volume of hypoxic waters commonly defined by $60\,\mu\mathrm{mol/kg}$) in the Indian Ocean, whereas the contraction is restricted to the very low oxygen levels found in the OMZ core in the Pacific Ocean (typically

535 volume with oxygen less than 10 to $20\,\mu\mathrm{mol/kg}$; Fig. 12~~a-b~~a,b). The oxygen gain in the southwest Indian Ocean is associated with an oxygen loss in the southeast. This dipole of southwest oxygenation and southeast deoxygenation along the path of the South Equatorial Current explains the redistribution regime and near zero ~~volume change of the OMZ~~ change of volumes delimited by intermediate oxygen levels (85 to $180\,\mu\mathrm{mol/kg}$; Fig. 12b). Finally, upstream of the South Equatorial Current, the drastic decline in oxygen ~~in~~ supplied by the water masses that enter the thermocline through the South Indian Gyre and

540 Indonesian Throughflow explains the expansion of ~~OMZ~~ volumes defined by high oxygen levels ($>180\,\mu\mathrm{mol/kg}$; Fig. 12a). The slowdown of the Southern Pathway is likely driven either by a weakening of Indian Central Water or Subantarctic Mode Water formation, but we do not disentangle these two effects in this study.

4.2 Beyond "single-pipe" and "mixing-network": cases for "two-pipe" and "moving pipe" systems

The projected oxygenation outside of the Indian OMZ core, or shadow zone, calls for a revision of the "single-pipe" and

545 "mixing-network" ventilation framework used in the Pacific Ocean (Gnanadesikan et al., 2007). In the original framework, increased ventilation and oxygenation with weakened circulation was only reconcilable in shadow zones where there are no direct advective ventilation pathways and a mixing-network of multiple sources controls ventilation. In both the Pacific and the Indian Oceans, the oxygenation of the OMZ core (which is associated with increased ventilation and reduced ideal age) can indeed be interpreted as a shift towards a stronger contribution from younger, oxygen-rich upper ocean waters using the

550 mixing-network model (Bryan et al., 2006; Gnanadesikan et al., 2007, 2012; Takano et al., 2018; Busecke et al., 2022). In the Pacific, this effect has been attributed to a slowdown of Deep Waters upwelling to thermocline depths, and there is evidence of this same effect in the Indian Ocean basin. In the ESM ensemble used in this study, upwelling of Deep Waters across 1000 m weakens at a rate of $2.0\pm0.7\,\mathrm{Sv/century}$ in the Indian Ocean, even reversing sign to be net downwelling (under SSP5-8.5 forcing in this ESM ensemble, see Fig. ~~S10~~S12).
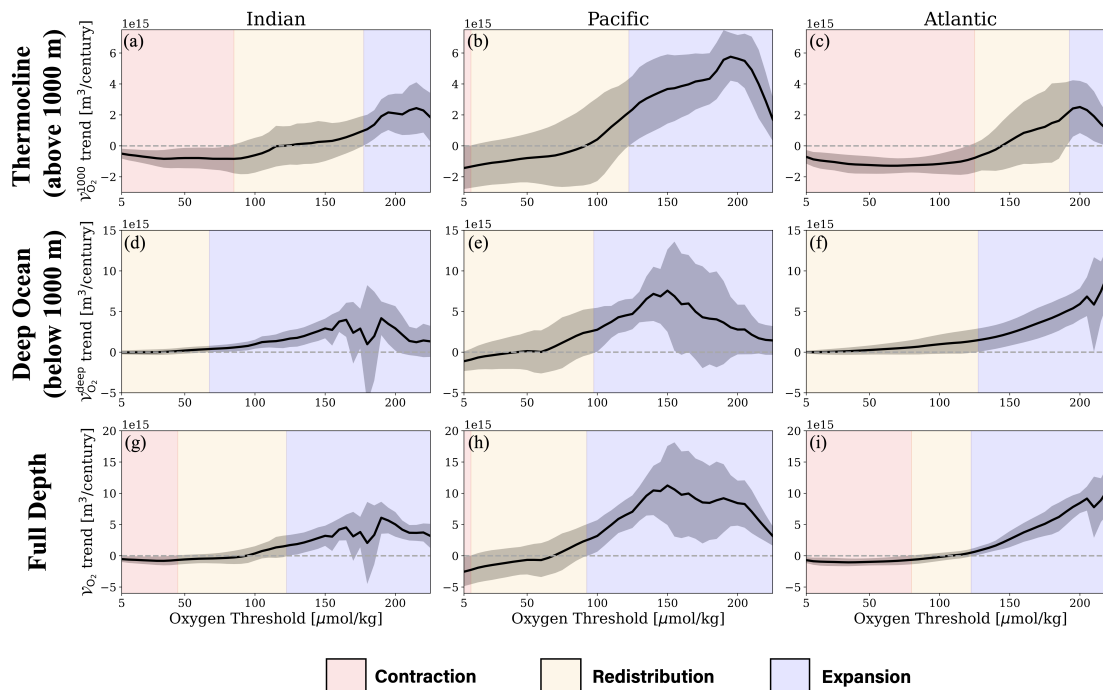
Figure 12. Multi-model mean thermocline OMZ volume trends (above 1000 m) under SSP5-8.5 scenario forcing (2015-2100) as a function of oxygen threshold for the tropical (30° S - 30° N) **(a)** Indian, **(b)** Pacific and **(c)** Atlantic Oceans. Deep ocean (below 1000 m) OMZ volume trends for the tropical **(d)** Indian, **(e)** Pacific and **(c)** Atlantic Oceans. Full depth OMZ volume trends for the tropical **(g)** Indian, **(h)** Pacific and **(i)** Atlantic Oceans. Shading represents one standard deviation of model spread from the mean. Panel a is the same as ~~Figure~~ Fig. 3a

555   Changes in mixing in the OMZ core are, however, not the primary effect driving oxygenation in the Indian Ocean. In the Southern Indian Ocean, ESMs project an oxygenation and increased ventilation well outside of the shadow zone, within regions of strong advection such as the South Equatorial Current. We show that this oxygenation can be interpreted as a "two-pipe" system, an intermediate case between a "single-pipe" and a "mixing-network". Two sources with different oxygen levels, rather than a network of many sources, are in fact sufficient to have increased oxygenation, even though the transport by both

560   ventilation sources weaken. The unique configuration of the Indonesian Throughflow and Southern Pathway merging into the South Equatorial Current allows for this phenomenon despite intense advection. The ventilation by the Southern Pathway and Indonesian Throughflow both decline in response to warming in the ESM ensemble, but the ventilation by the Indonesian Throughflow declines more strongly, favoring the relative contribution of the better oxygenated Southern Pathway waters.

Another feature of the Indian Ocean OMZ response which differs from its Pacific Ocean counterpart is the importance of

565   ventilation by marginal sea outflows. We find that changes in ventilation from marginal sea outflows ~~are the main control~~ may be a significant driver of deoxygenation in the Arabian Sea. The Persian Gulf rapidly warms in response to global warming, increasing stratification and the buoyancy of outflow water from the Persian Gulf. As outflow water shoals, it becomes unable

26

to ventilate the OMZ in the Arabian Sea, and is instead confined to the upper 100 m where its impact on oxygen becomes marginal (the upper ocean is already well oxygenated; Lachkar et al., 2021). The deeper Red Sea outflow plume also shows
570 evidence of shoaling in the ESM ensemble, but it has a weaker impact on the ventilation of the OMZ because its oxygen content is lower than that of the Persian Gulf (on average about $70\,\mu\text{mol/kg}$ for Red Sea Outflow Water versus about $200\,\mu\text{mol/kg}$ for Persian Gulf Water). We can describe this change in the ventilation from marginal seas as a "moving pipe", where oxygen supply may be affected by a displacement of a pathway even if the strength of transport along a that pathway holds steady.

4.3 Global trends in tropical oxygen minimum zones

575 Now extending our scope to all tropical oceans, we find that the three-regime OMZ response identified in the Indian (this study) and Pacific (Busecke et al., 2022) Oceans is also simulated in the Atlantic Ocean (Fig. 12c, S19). The dynamics driving this three-regime response in the Atlantic have not yet been explored in detail, but it is likely that the even more prominent contraction regime found for the Atlantic OMZ is connected to changes in ventilation by the Atlantic ~~Meridional Overturning~~ meridional overturning circulation, which is projected to weaken in ESMs (IPCC et al., 2013; Bakker et al., 2016). This would
580 lead to a favoring of midlatitude waters from the south, as South Atlantic Mode and Intermediate water subduction rates are projected to hold steady and ventilate lighter densities (Goes et al., 2008; Downes et al., 2009). Looking beyond OMZ volume changes in the ocean thermocline (above 1000 m) to the deep ocean response (below 1000 m), we see that deoxygenation and OMZ expansion in the deep ocean are more ubiquitous than in the thermocline (Fig. 12d-f). Deoxygenation in the deep ocean is likely due to a slowdown of Deep Water transports as the global thermohaline circulation weakens with warming (e.g. Bakker
585 et al., 2016). When integrating the thermocline and deep ocean components of the OMZ response to consider the full depth of the water column (similar to what was done for the Pacific Ocean in Busecke et al., 2022), we find that the thermocline response dominates the OMZ contraction at low oxygen thresholds while the deep ocean response dominates the expansion at high thresholds (Fig. 12g-i).

4.4 Observational constraints, limitations and caveats

590 Projected oxygen changes, and thus OMZ volume changes are subject to uncertainties, in particular the magnitude of the oxygenation/deoxygenation dipole along the South Equatorial Current and the deoxygenation in the northern Arabian Sea. The slowdown of the Southern Pathway and Indonesian Throughflow transports is a robust and well studied feature of ESM projections (Downes et al., 2009; Sen Gupta et al., 2016; Feng et al., 2017; Stellema et al., 2019). The pattern of multi-model mean oxygen trends (Fig. 4) is not sensitive to our model selection protocol, as the three features are also simulated by the six
595 ESMs excluded from the ensemble (Fig. S8). However, when all 14 available ESMs are included in the multi-model mean, we find that the deoxygenation in Features 1 and 3 are enhanced, while the oxygenation in Feature 3 is weakened (Fig. S9).

Historical observations support the slowdown and deoxygenation of the Southern Pathway (Helm et al., 2011; Kobayashi et al., 2012; Ito et al., 2017; McMonigal et al., 2022). A secular weakening of the Indonesian Throughflow has not yet been observed, possibly obscured by significant decadal variability (Liu et al., 2015; Feng et al., 2018), but there is evidence for forced
600 trends in the global thermohaline circulation that controls the Indonesian Throughflow transport ~~(Rahmstorf et al., 2015)~~

(Rahmstorf et al., 2015; Sun and Thompson, 2020) to support the decline in ventilation by this pathway. However, the relative changes in the two pathways, which controls the oxygenation/deoxygenation dipole, is highly uncertain and unconstrained by observations. This dipole pattern has not emerged in current observation-based estimates of historical oxygen trends (Helm et al., 2011; Ito et al., 2017; Schmidtko et al., 2017), though there is some signal of oxygenation near Madagascar in the product of Ito et al. (2017). A detailed study on the time of emergence of oxygen and volume trends identified in this work would require greater availability of large ensembles with biogeochemistry in future generations of CMIP.

Deoxygenation in the northern Arabian Sea has been detected in observations (reviewed by Lachkar et al., 2023). The rapid heating of marginal seas compared to the open ocean and the subsequent increase in stratification and buoyancy of the marginal sea outflows, particularly for the Persian Gulf, is also supported by observations (Al-Yamani et al., 2017; Naqvi, 2021). The projected changes in outflow ventilation are consistent with the findings of ocean model simulation studies, which showed that the warming and shoaling of the Persian Gulf was a major driver of the deoxygenation in the northern Arabian Sea (Lachkar et al., 2019, 2021). Yet, ESMs tend to overestimate the oxygen transport by these marginal sea outflows to the Arabian Sea (e.g. Schmidt et al., 2021, for CMIP5). This partially explains the systematic high oxygen bias in the Arabian Sea in the ensemble of eight CMIP6 ESMs used in this study (Fig. 1), the absence of ~~an OMZ core~~ a suboxia in the five ESMs that were excluded from the ensemble (~~Fig.~~ Table S1~~,S2~~), and could influence the magnitude of the projected deoxygenation associated with the vertical displacement of these outflows. In fact, a study by Vallivattathillam et al. (2023), which applies downscaling methods to CMIP5 projections of Arabian Sea oxygen under the high emission RCP8.5 forcing, finds that the deoxygenation simulated in CMIP5 models in the region is not preserved after the bias-corrected downscaling method is applied (averaging between 200 and 700 m). This suggests that ESM simulated mean state biases in the Arabian Sea can have a profound impact on the projected changes.

An additional challenge of the Optimum Multiparameter (OMP) analysis is to distinguish between changes due to source water types and changes in mixing with surface waters. Specifically in the Arabian Sea, Persian Gulf Water and Arabian Sea surface water both tend to be anomalously warm, saline and well oxygenated. Thus, it is possible that increased stratification and weakened vertical exchange with the surface is interpreted as a decrease in Persian Gulf Water fraction in the OMP. The presence of Northern Arabian Sea deoxygenation in MIROC-ES2L, an ESM which does not resolve the marginal seas and was thus excluded from the OMP analysis for the region, also suggests that stratification increases may play a first-order role in Northern Arabian Sea deoxygenation in the ESM ensemble. This is also consistent with a previous study by Lachkar et al. (2021), which investigates deoxygenation in the Arabian Sea from 1982 to 2010 using a high-resolution regional ocean model, and attributes about 75 % of ventilation decreases over this period to vertical mixing changes and only 25 % to advective changes. We note that the compensation between the effects of export and stratification changes may in fact be key to allowing the OMP model to perform well in this region.

Further work, including for example a full oxygen budget analysis or lagrangian particle tracking, would be required to better disentangle the effects of marginal sea shoaling and increased stratification in the projections of Arabian Sea oxygen for the ESMs used in this study; however, data for such a study are not currently available. Based on these considerations, the relative effects of marginal sea shoaling and increased stratification in ESM projections of the northern Arabian Sea remain

largely uncertain. Ultimately though, the present study supports the conclusions of the recent review by Lachkar et al. (2023): the Arabian Sea OMZ will be reshaped by changes in stratification and the Persian Gulf outflow driving deoxygenation in the northern subsurface layer, while increased ventilation from the south drives oxygenation of the deeper layers.

5 Conclusion

640 Oxygen minimum zones can be viewed as multiple concentric layers, like onions, with oxygen concentrations decreasing towards their core. Their response to deoxygenation and global warming in Earth system models falls into three regimes which are controlled by the mechanisms that ventilate these different layers: the outer layers of the oxygen minimum zone expand, the inner layers contract, and in-between, oxygen is redistributed leading to near zero changes in volume but reshaping the spatial distribution of the intermediate layers. We show that this contrast between inner layer oxygenation and outer layer

645 deoxygenation, which was first identified in the Pacific Ocean (e.g., Gnanadesikan et al., 2007; Busecke et al., 2022), applies to all tropical oxygen minimum zones. However, the unique geometry and ventilation pathways of the tropical Indian Ocean (bounded by continent to the north, Indonesian Throughflows and marginal seas) determine what layers of the oxygen minimum zone experience contraction, redistribution and expansion. The Indian Ocean is characterized by a prominent oxygenation, attributed to changes in the ventilation by the Indonesian Throughflow, and consequently contraction and redistribution regimes

650 that extend to a much larger range of oxygen minimum zone layers than its Pacific counterpart. Furthermore, the rapid warming and shoaling of marginal sea outflows leads to localized deoxygenation in the inner layers of the oxygen minimum zone of the northern Arabian Sea. We identify that the response of the Atlantic oxygen minimum zone also exhibits regimes of contraction, redistribution, and expansion, but further investigations are required to understand the regional dynamics which produce a pronounced contraction response in that basin.

655 *Code and data availability.* The processed data files and code to reproduce results presented here are available at https://doi.org/10.5281/zenodo.8342233

Appendix A: Extended Optimum Multiparameter Analysis

Extended Optimum Multiparameter Analysis (OMP; Karstensen and Tomczak, 1998) is a method of solving an over-determined linear ~~mixing~~ mixture model which takes into account the conversion of one tracer to another, generally by remineralization. Detailed explanations of the OMP method can be found in Tomczak and Large (1989) and Shrikumar et al. (2022), but here

660 we give a brief summary.

First, we define a set of N source water masses with properties, p. Let e_p^i be the values for property p and i-th source water mass. Each sample in the evaluation region has a value for each property, s_p^j. The goal is to solve for the fraction of i-th source

water masses in each sample, x_i^j. We can define the objective function:

$$\sum_{i=1}^{N} e_p^i x_i^j = s_p^j + \epsilon_p^j \tag{A1}$$

where ϵ_p^j is a residual to minimize. Using user defined weights, W, to assign relative importance to each property, the residual takes the form

$$\epsilon_p^j = \frac{W_p}{\sigma_p} W_p \Big(\sum_i (e_p^i - \mu_p) x_i^j + r_B^A \Delta_j^B - (s_p^j - \mu_p) \Big) \tag{A2}$$

where we ~~normalize and~~ center the values for each property, e_p^i with their mean, μ_p~~, and variance, σ_p.~~. The user defined weights play the role of normalizing across fields. We chose to set ~~potential temperature and salinity fields weighted five times higher than dissolved oxygen fields in the mixing model's objective function because~~ weight for dissolved oxygen and AOU at 2 % the weight of potential temperature and salinity ~~tend to be the defining characteristics for source water masses~~ fields to account for the greater range of values in sources of dissolved oxygen. The results of the analysis are not sensitive to small changes in weight values. The term $r_B^A \Delta_j^B$ allows for the conservation of two properties, A and B, which are exchanged via remineralization. Typically, this term is used to track conversion of oxygen to phosphorous, where r is set to be the Redfield Ratio. In this study, we simply allow for the conversion of oxygen to AOU with a ratio of -1. The cost function is thus defined as the sum of residuals for every property, p, as well as a mass conservation term ϵ_M^j which penalizes deviations from total mass fractions of unity for each sample point:

$$C^j = (\epsilon_M^j)^2 + \sum_p (\epsilon_p^j)^2 \tag{A3}$$

We note that the PyOMPA implementation of this method allows for a hard constraint on mass conservation, rather than minimizing a residual (Shrikumar et al., 2022). However, we do not use this feature, and thus recover the original method of Karstensen and Tomczak (1998).

Appendix B: ~~Interpreting Pearson Correlations between AOU and Ideal Age anomalies~~

~~The Pearson Correlation Coefficient is a measure of linear correlation between two variables. Thus, for fields x and y related by the form $y = mx + \mathcal{N}$ for some constant m and noise $\mathcal{N}$, the correlation coefficient is 1 if $\mathcal{N} = 0$.~~

~~Here, we derive the form of the noise term $\mathcal{N}$ for the linear relation between AOU and ideal age for a parcel of water. We assume the parcel of water can be made up of contributions from N ventilation pathways, each with an average respiration rate R, ideal age τ, and fractional contribution to the mass of the parcel f. AOU and ideal age of the parcel is thus modeled as:~~

$$\overline{AOU} = \overline{R\tau} = \sum_i^N f_i R_i \tau_i$$

$$\overline{\tau} = \sum_i^N f_i \tau_i$$

690 Changes in AOU and ideal age are modeled as

$$\Delta\overline{AOU} = \sum_i^N (\Delta f_i R_i \tau_i + f_i \Delta R_i \tau_i + f_i R_i \Delta\tau_i)$$

$$\Delta\overline{\tau} = \sum_i^N (\Delta f_i \tau_i + f_i \Delta\tau_i)$$

Rearranging,

$$\Delta\overline{AOU} = \sum_i^N (\Delta f_i R_i \tau_i + f_i R_i \Delta\tau_i + f_i \Delta R_i \tau_i)$$

695

$$= \sum_i^N R_i \sum_i^N (\Delta f_i \tau_i + f_i \Delta\tau_i) - \sum_{i\neq j}^N f_j R_i \Delta\tau_j - \sum_{i\neq j}^N \Delta f_j R_i \tau_j + \sum_i^N f_i \Delta R_i \tau_i$$

$$= \Delta\overline{\tau} \sum_i^N R_i - \sum_{i\neq j}^N f_j R_i \Delta\tau_j - \sum_{i\neq j}^N \Delta f_j R_i \tau_j + \sum_i^N f_i \Delta R_i \tau_i$$

Thus, we can relate AOU and ideal age changes of the parcel in the form $\Delta\overline{AOU} = m\Delta\overline{\tau} + \mathcal{N}$, where

$$m = \sum_i^N R_i$$

and

700
$$\mathcal{N} = \sum_i^N f_i \Delta R_i \tau_i - \sum_{i\neq j}^N (f_j R_i \Delta\tau_j + \Delta f_j R_i \tau_j)$$

The two terms in $\mathcal{N}$ respectively represent changes in respiration rates along each pathway and a loss of information on constituent pathways in the averaged signal. So, a correlation coefficient of 1 between AOU and ideal age changes represent the special case where changes occur along a single pathway and respiration rates remain constant.

References

Abernathey, R. P., Busecke, J. J. M., Smith, T. A., Deauna, J. D., Banihirwe, A., Nicholas, T., Fernandes, F., James, B., Dussin, R., Cherian, D. A., Caneill, R., Sinha, A., Uieda, L., Rath, W., Balwada, D., Constantinou, N. C., Ponte, A., Zhou, Y., Uchida, T., and Thielen, J.: xgcm, https://doi.org/10.5281/zenodo.7348619, 2022.

Al Azhar, M., Lachkar, Z., Lévy, M., and Smith, S.: Oxygen minimum zone contrasts between the Arabian Sea and the Bay of Bengal implied by differences in remineralization depth, Geophysical Research Letters, 44, 11–106, 2017.

Al-Yamani, F., Yamamoto, T., Al-Said, T., and Alghunaim, A.: Dynamic hydrographic variations in northwestern Arabian Gulf over the past three decades: Temporal shifts and trends derived from long-term monitoring data, Marine Pollution Bulletin, 122, 488–499, 2017.

Auderset, A., Moretti, S., Taphorn, B., Ebner, P.-R., Kast, E., Wang, X. T., Schiebel, R., Sigman, D. M., Haug, G. H., and Martínez-García, A.: Enhanced ocean oxygenation during Cenozoic warm periods, Nature, 609, 77–82, 2022.

Bakker, P., Schmittner, A., Lenaerts, J., Abe-Ouchi, A., Bi, D., van den Broeke, M., Chan, W.-L., Hu, A., Beadling, R., Marsland, S., et al.: Fate of the Atlantic Meridional Overturning Circulation: Strong decline under continued warming and Greenland melting, Geophysical Research Letters, 43, 12–252, 2016.

Banse, K., Naqvi, S., Narvekar, P., Postel, J., and Jayakumar, D.: Oxygen minimum zone of the open Arabian Sea: variability of oxygen and nitrite from daily to decadal timescales, Biogeosciences, 11, 2237–2261, 2014.

Beal, L. M., Ffield, A., and Gordon, A. L.: Spreading of Red Sea overflow waters in the Indian Ocean, Journal of Geophysical Research: Oceans, 105, 8549–8564, 2000.

Bentsen, M., Oliviè, D. J. L., Seland, y., Toniazzo, T., Gjermundsen, A., Graff, L. S., Debernard, J. B., Gupta, A. K., He, Y., Kirkevåg, A., Schwinger, J., Tjiputra, J., Aas, K. S., Bethke, I., Fan, Y., Griesfeller, J., Grini, A., Guo, C., Ilicak, M., Karset, I. H. H., Landgren, O. A., Liakka, J., Moseid, K. O., Nummelin, A., Spensberger, C., Tang, H., Zhang, Z., Heinze, C., Iversen, T., and Schulz, M.: NCC NorESM2-MM model output prepared for CMIP6 CMIP, https://doi.org/10.22033/ESGF/CMIP6.506, 2019a.

Bentsen, M., Oliviè, D. J. L., Seland, y., Toniazzo, T., Gjermundsen, A., Graff, L. S., Debernard, J. B., Gupta, A. K., He, Y., Kirkevåg, A., Schwinger, J., Tjiputra, J., Aas, K. S., Bethke, I., Fan, Y., Griesfeller, J., Grini, A., Guo, C., Ilicak, M., Karset, I. H. H., Landgren, O. A., Liakka, J., Moseid, K. O., Nummelin, A., Spensberger, C., Tang, H., Zhang, Z., Heinze, C., Iversen, T., and Schulz, M.: NCC NorESM2-MM model output prepared for CMIP6 ScenarioMIP, https://doi.org/10.22033/ESGF/CMIP6.608, 2019b.

Bertrand, A., Chaigneau, A., Peraltilla, S., Ledesma, J., Graco, M., Monetti, F., and Chavez, F. P.: Oxygen: a fundamental property regulating pelagic ecosystem structure in the coastal southeastern tropical Pacific, PloS one, 6, e29558, 2011.

Bindoff, N. L., Cheung, W. W., Kairo, J. G., Arístegui, J., Guinder, V. A., Hallberg, R., Hilmi, N. J. M., Jiao, N., Karim, M. S., Levin, L., et al.: Changing ocean, marine ecosystems, and dependent communities, IPCC special report on the ocean and cryosphere in a changing climate, pp. 477–587, 2019.

Bopp, L., Resplandy, L., Orr, J. C., Doney, S. C., Dunne, J. P., Gehlen, M., Halloran, P., Heinze, C., Ilyina, T., Seferian, R., et al.: Multiple stressors of ocean ecosystems in the 21st century: projections with CMIP5 models, Biogeosciences, 10, 6225–6245, 2013.

Bopp, L., Resplandy, L., Untersee, A., Le Mezo, P., and Kageyama, M.: Ocean (de) oxygenation from the Last Glacial Maximum to the twenty-first century: insights from Earth System models, Philosophical Transactions of the Royal Society A: Mathematical, Physical and Engineering Sciences, 375, 20160323, 2017.

Bouchard, C. and Crumplin, W.: Neglected no longer: the Indian Ocean at the forefront of world geopolitics and global geostrategy, Journal of the Indian Ocean Region, 6, 26–51, 2010.

Brandt, P., Bange, H. W., Banyte, D., Dengler, M., Didwischus, S.-H., Fischer, T., Greatbatch, R. J., Hahn, J., Kanzow, T., Karstensen, J., et al.: On the role of circulation and mixing in the ventilation of oxygen minimum zones with a focus on the eastern tropical North Atlantic, Biogeosciences, 12, 489–512, 2015.

Brill, R. W.: Selective advantages conferred by the high performance physiology of tunas, billfishes, and dolphin fish, Comparative Biochemistry and Physiology Part A: Physiology, 113, 3–15, 1996.

Bryan, F. O., Danabasoglu, G., Gent, P. R., and Lindsay, K.: Changes in ocean ventilation during the 21st century in the CCSM3, Ocean Modelling, 15, 141–156, 2006.

Busecke, J. J., Resplandy, L., Ditkovsky, S. J., and John, J. G.: Diverging fates of the Pacific Ocean oxygen minimum zone and its core in a warming world, AGU Advances, 3, e2021AV000 470, 2022.

Busecke, J. J. M. and Spring, A.: jbusecke/cmip6_preprocessing: v0.1.4, https://doi.org/10.5281/zenodo.3743397, 2020.

Cabré, A., Marinov, I., Bernardello, R., and Bianchi, D.: Oxygen minimum zones in the tropical Pacific across CMIP5 models: mean state differences and climate change trends, Biogeosciences, 12, 5429–5454, 2015.

Christian, J. R., Denman, K. L., Hayashida, H., Holdsworth, A. M., Lee, W. G., Riche, O. G., Shao, A. E., Steiner, N., and Swart, N. C.: Ocean biogeochemistry in the Canadian Earth system model version 5.0. 3: CanESM5 and CanESM5-CanOE, Geoscientific Model Development, 15, 4393–4424, 2022.

Clifton, J., Etienne, M., Barnes, D. K., Barnes, R. S., Suggett, D. J., and Smith, D. J.: Marine conservation policy in Seychelles: Current constraints and prospects for improvement, Marine Policy, 36, 823–831, 2012.

Cocco, V., Joos, F., Steinacher, M., Frölicher, T. L., Bopp, L., Dunne, J., Gehlen, M., Heinze, C., Orr, J., Oschlies, A., et al.: Oxygen and indicators of stress for marine life in multi-model global warming projections, Biogeosciences, 10, 1849–1868, 2013.

Deutsch, C., Berelson, W., Thunell, R., Weber, T., Tems, C., McManus, J., Crusius, J., Ito, T., Baumgartner, T., Ferreira, V., et al.: Centennial changes in North Pacific anoxia linked to tropical trade winds, Science, 345, 665–668, 2014.

Deutsch, C., Penn, J. L., and Seibel, B.: Metabolic trait diversity shapes marine biogeography, Nature, 585, 557–562, 2020.

Downes, S. M., Bindoff, N. L., and Rintoul, S. R.: Impacts of climate change on the subduction of mode and intermediate water masses in the Southern Ocean, Journal of Climate, 22, 3289–3302, 2009.

Dueri, S.: Impacts of climate change and ocean acidification on Indian Ocean tunas, IDDRI, Report in" Impacts of climate change and ocean acidification on Indian Ocean tunas, 2017.

Dueri, S., Bopp, L., and Maury, O.: Projecting the impacts of climate change on skipjack tuna abundance and spatial distribution, Global Change Biology, 20, 742–753, 2014.

Dunne, J. P., Horowitz, L., Adcroft, A., Ginoux, P., Held, I., John, J., Krasting, J. P., Malyshev, S., Naik, V., Paulot, F., et al.: The GFDL Earth System Model version 4.1 (GFDL-ESM 4.1): Overall coupled model description and simulation characteristics, Journal of Advances in Modeling Earth Systems, 12, e2019MS002 015, 2020.

Duteil, O., Böning, C. W., and Oschlies, A.: Variability in subtropical-tropical cells drives oxygen levels in the tropical Pacific Ocean, Geophysical Research Letters, 41, 8926–8934, 2014.

Duteil, O., Frenger, I., and Getzlaff, J.: The riddle of eastern tropical Pacific Ocean oxygen levels: the role of the supply by intermediate-depth waters, Ocean Science, 17, 1489–1507, 2021.

Eyring, V., Bony, S., Meehl, G. A., Senior, C. A., Stevens, B., Stouffer, R. J., and Taylor, K. E.: Overview of the Coupled Model Intercomparison Project Phase 6 (CMIP6) experimental design and organization, Geoscientific Model Development, 9, 1937–1958, 2016.

790   Feng, M., Zhang, X., Sloyan, B., and Chamberlain, M.: Contribution of the deep ocean to the centennial changes of the Indonesian Through-
flow, Geophysical Research Letters, 44, 2859–2867, 2017.

Feng, M., Zhang, N., Liu, Q., and Wijffels, S.: The Indonesian throughflow, its variability and centennial change, Geoscience Letters, 5,
1–10, 2018.

Fine, R. A.: Circulation of Antarctic intermediate water in the South Indian Ocean, Deep Sea Research Part I: Oceanographic Research
795   Papers, 40, 2021–2042, 1993.

Firing, E., Fernandes, F., Barna, A., and Abernathey, R.: GSW-python: Python implementation of the Thermodynamic Equation of Seawater
2010 (TEOS-10), Zenodo [code], 2021.

Garcia, H., Weathers, K., Paver, C., Smolyar, I., Boyer, T., Locarnini, M., Zweng, M., Mishonov, A., Baranova, O., Seidov, D., et al.: World
Ocean Atlas 2018, Volume 3: Dissolved Oxygen, Apparent Oxygen Utilization, and Dissolved Oxygen Saturation., 2019.

800   Gattuso, J.-P., Magnan, A., Billé, R., Cheung, W. W., Howes, E. L., Joos, F., Allemand, D., Bopp, L., Cooley, S. R., Eakin, C. M., et al.:
Contrasting futures for ocean and society from different anthropogenic CO2 emissions scenarios, Science, 349, aac4722, 2015.

Gnanadesikan, A., Russell, J., and Zeng, F.: How does ocean ventilation change under global warming?, Ocean Science, 3, 43–53, 2007.

Gnanadesikan, A., Dunne, J., and John, J.: Understanding why the volume of suboxic waters does not increase over centuries of global
warming in an Earth System Model, Biogeosciences, 9, 1159–1172, 2012.

805   Gnanadesikan, A., Bianchi, D., and Pradal, M.-A.: Critical role for mesoscale eddy diffusion in supplying oxygen to hypoxic ocean waters,
Geophysical Research Letters, 40, 5194–5198, 2013.

Goes, M., Wainer, I., Gent, P. R., and Bryan, F. O.: Changes in subduction in the South Atlantic Ocean during the 21st century in the CCSM3,
Geophysical Research Letters, 35, 2008.

Good, P., Sellar, A., Tang, Y., Rumbold, S., Ellis, R., Kelley, D., Kuhlbrodt, T., and Walton, J.: MOHC UKESM1.0-LL model output prepared
810   for CMIP6 ScenarioMIP, https://doi.org/10.22033/ESGF/CMIP6.1567, 2019.

Guo, H., John, J. G., Blanton, C., McHugh, C., Nikonov, S., Radhakrishnan, A., Rand, K., Zadeh, N. T., Balaji, V., Durachta, J., Dupuis, C.,
Menzel, R., Robinson, T., Underwood, S., Vahlenkamp, H., Bushuk, M., Dunne, K. A., Dussin, R., Gauthier, P. P., Ginoux, P., Griffies,
S. M., Hallberg, R., Harrison, M., Hurlin, W., Lin, P., Malyshev, S., Naik, V., Paulot, F., Paynter, D. J., Ploshay, J., Reichl, B. G.,
Schwarzkopf, D. M., Seman, C. J., Shao, A., Silvers, L., Wyman, B., Yan, X., Zeng, Y., Adcroft, A., Dunne, J. P., Held, I. M., Krast-
815   ing, J. P., Horowitz, L. W., Milly, P., Shevliakova, E., Winton, M., Zhao, M., and Zhang, R.: NOAA-GFDL GFDL-CM4 model output,
https://doi.org/10.22033/ESGF/CMIP6.1402, 2018a.

Guo, H., John, J. G., Blanton, C., McHugh, C., Nikonov, S., Radhakrishnan, A., Rand, K., Zadeh, N. T., Balaji, V., Durachta, J., Dupuis,
C., Menzel, R., Robinson, T., Underwood, S., Vahlenkamp, H., Dunne, K. A., Gauthier, P. P., Ginoux, P., Griffies, S. M., Hallberg,
R., Harrison, M., Hurlin, W., Lin, P., Malyshev, S., Naik, V., Paulot, F., Paynter, D. J., Ploshay, J., Schwarzkopf, D. M., Seman, C. J.,
820   Shao, A., Silvers, L., Wyman, B., Yan, X., Zeng, Y., Adcroft, A., Dunne, J. P., Held, I. M., Krasting, J. P., Horowitz, L. W., Milly, C.,
Shevliakova, E., Winton, M., Zhao, M., and Zhang, R.: NOAA-GFDL GFDL-CM4 model output prepared for CMIP6 ScenarioMIP,
https://doi.org/10.22033/ESGF/CMIP6.9242, 2018b.

Hajima, T., Abe, M., Arakawa, O., Suzuki, T., Komuro, Y., Ogura, T., Ogochi, K., Watanabe, M., Yamamoto, A., Tatebe, H., Noguchi, M. A.,
Ohgaito, R., Ito, A., Yamazaki, D., Ito, A., Takata, K., Watanabe, S., Kawamiya, M., and Tachiiri, K.: MIROC MIROC-ES2L model output
825   prepared for CMIP6 CMIP, https://doi.org/10.22033/ESGF/CMIP6.902, 2019.

Harper, S.: Thermocline ventilation and pathways of tropical–subtropical water mass exchange, Tellus A: Dynamic Meteorology and
Oceanography, 52, 330–345, 2000.

Held, I., Guo, H., Adcroft, A., Dunne, J., Horowitz, L., Krasting, J., Shevliakova, E., Winton, M., Zhao, M., Bushuk, M., et al.: Structure and performance of GFDL's CM4. 0 climate model, Journal of Advances in Modeling Earth Systems, 11, 3691–3727, 2019.

830 Helm, K. P., Bindoff, N. L., and Church, J. A.: Observed decreases in oxygen content of the global ocean, Geophysical Research Letters, 38, 2011.

IPCC, A. et al.: Climate change 2013: the physical science basis, Contribution of working group I to the fifth assessment report of the intergovernmental panel on climate change, 1535, 2013.

Ito, T., Minobe, S., Long, M. C., and Deutsch, C.: Upper ocean O2 trends: 1958–2015, Geophysical Research Letters, 44, 4214–4223, 2017.

835 John, J. G., Blanton, C., McHugh, C., Radhakrishnan, A., Rand, K., Vahlenkamp, H., Wilson, C., Zadeh, N. T., Dunne, J. P., Dussin, R., Horowitz, L. W., Krasting, J. P., Lin, P., Malyshev, S., Naik, V., Ploshay, J., Shevliakova, E., Silvers, L., Stock, C., Winton, M., and Zeng, Y.: NOAA-GFDL GFDL-ESM4 model output prepared for CMIP6 ScenarioMIP, https://doi.org/10.22033/ESGF/CMIP6.1414, 2018.

Jungclaus, J., Bittner, M., Wieners, K.-H., Wachsmann, F., Schupfner, M., Legutke, S., Giorgetta, M., Reick, C., Gayler, V., Haak, H., de Vrese, P., Raddatz, T., Esch, M., Mauritsen, T., von Storch, J.-S., Behrens, J., Brovkin, V., Claussen, M., Crueger, T., Fast, I., Fiedler,
840 S., Hagemann, S., Hohenegger, C., Jahns, T., Kloster, S., Kinne, S., Lasslop, G., Kornblueh, L., Marotzke, J., Matei, D., Meraner, K., Mikolajewicz, U., Modali, K., Müller, W., Nabel, J., Notz, D., Peters, K., Pincus, R., Pohlmann, H., Pongratz, J., Rast, S., Schmidt, H., Schnur, R., Schulzweida, U., Six, K., Stevens, B., Voigt, A., and Roeckner, E.: MPI-M MPIESM1.2-HR model output prepared for CMIP6 CMIP, https://doi.org/10.22033/ESGF/CMIP6.741, 2019.

Karstensen, J. and Quadfasel, D.: Water subducted into the Indian Ocean subtropical gyre, Deep Sea Research Part II: Topical Studies in
845 Oceanography, 49, 1441–1457, 2002.

Karstensen, J. and Tomczak, M.: Ventilation processes and water mass ages in the thermocline of the southeast Indian Ocean, Geophysical Research Letters, 24, 2777–2780, 1997.

Karstensen, J. and Tomczak, M.: Age determination of mixed water masses using CFC and oxygen data, Journal of Geophysical Research: Oceans, 103, 18 599–18 609, 1998.

850 Keeling, R. F., Körtzinger, A., Gruber, N., et al.: Ocean deoxygenation in a warming world, Annu. Rev. Mar. Sci, 2, 199–229, 2010.

Kobayashi, T., Mizuno, K., and Suga, T.: Long-term variations of surface and intermediate waters in the southern Indian Ocean along 32 S, Journal of oceanography, 68, 243–265, 2012.

Krasting, J. P., John, J. G., Blanton, C., McHugh, C., Nikonov, S., Radhakrishnan, A., Rand, K., Zadeh, N. T., Balaji, V., Durachta, J., Dupuis, C., Menzel, R., Robinson, T., Underwood, S., Vahlenkamp, H., Dunne, K. A., Gauthier, P. P., Ginoux, P., Griffies, S. M., Hallberg, R.,
855 Harrison, M., Hurlin, W., Malyshev, S., Naik, V., Paulot, F., Paynter, D. J., Ploshay, J., Reichl, B. G., Schwarzkopf, D. M., Seman, C. J., Silvers, L., Wyman, B., Zeng, Y., Adcroft, A., Dunne, J. P., Dussin, R., Guo, H., He, J., Held, I. M., Horowitz, L. W., Lin, P., Milly, P., Shevliakova, E., Stock, C., Winton, M., Wittenberg, A. T., Xie, Y., and Zhao, M.: NOAA-GFDL GFDL-ESM4 model output prepared for CMIP6 CMIP, https://doi.org/10.22033/ESGF/CMIP6.1407, 2018.

Kwiatkowski, L., Torres, O., Bopp, L., Aumont, O., Chamberlain, M., Christian, J. R., Dunne, J. P., Gehlen, M., Ilyina, T., John, J. G., et al.:
860 Twenty-first century ocean warming, acidification, deoxygenation, and upper-ocean nutrient and primary production decline from CMIP6 model projections, Biogeosciences, 17, 3439–3470, 2020.

Lachkar, Z., Smith, S., Lévy, M., and Pauluis, O.: Eddies reduce denitrification and compress habitats in the Arabian Sea, Geophysical Research Letters, 43, 9148–9156, 2016.

Lachkar, Z., Lévy, M., and Smith, K. S.: Strong intensification of the Arabian Sea oxygen minimum zone in response to Arabian Gulf
865 warming, Geophysical Research Letters, 46, 5420–5429, 2019.

Lachkar, Z., Mehari, M., Al Azhar, M., Lévy, M., and Smith, S.: Fast local warming is the main driver of recent deoxygenation in the northern Arabian Sea, Biogeosciences, 18, 5831–5849, 2021.

Lachkar, Z., Lévy, M., Hailegeorgis, D., and Vallivattathillam, P.: Differences in recent and future trends in the Arabian Sea oxygen minimum zone: processes and uncertainties, Frontiers in Marine Science, 10, 1122 043, 2023.

870 Levin, L. A.: Manifestation, drivers, and emergence of open ocean deoxygenation, Annual review of marine science, 10, 229–260, 2018.

Lévy, M., Resplandy, L., Palter, J. B., Couespel, D., and Lachkar, Z.: The crucial contribution of mixing to present and future ocean oxygen distribution, in: Ocean mixing, pp. 329–344, Elsevier, 2022.

Liu, Q.-Y., Feng, M., Wang, D., and Wijffels, S.: Interannual variability of the I ndonesian T hroughflow transport: A revisit based on 30 year expendable bathythermograph data, Journal of Geophysical Research: Oceans, 120, 8270–8282, 2015.

875 Llanillo, P., Pelegrí, J. L., Talley, L., Peña-Izquierdo, J., and Cordero, R.: Oxygen pathways and budget for the eastern South Pacific oxygen minimum zone, Journal of Geophysical Research: Oceans, 123, 1722–1744, 2018.

Llewellyn, L. E., English, S., and Barnwell, S.: A roadmap to a sustainable Indian Ocean blue economy, Journal of the Indian Ocean Region, 12, 52–66, 2016.

Luyten, J., Pedlosky, J., and Stommel, H.: The ventilated thermocline, Journal of Physical Oceanography, 13, 292–309, 1983.

880 Margolskee, A., Frenzel, H., Emerson, S., and Deutsch, C.: Ventilation pathways for the North Pacific oxygen deficient zone, Global Biogeochemical Cycles, 33, 875–890, 2019.

McCarthy, M. C. and Talley, L. D.: Three-dimensional isoneutral potential vorticity structure in the Indian Ocean, Journal of Geophysical Research: Oceans, 104, 13 251–13 267, 1999.

McCarthy, M. C., Talley, L. D., and Baringer, M. O.: Deep upwelling and diffusivity in the southern Central Indian Basin, Geophysical
885 Research Letters, 24, 2801–2804, 1997.

McMonigal, K., Gunn, K. L., Beal, L. M., Elipot, S., and Willis, J. K.: Reduction in meridional heat export contributes to recent Indian Ocean warming, Journal of physical oceanography, 52, 329–345, 2022.

Menezes, V. V.: Advective pathways and transit times of the Red Sea Overflow Water in the Arabian Sea from Lagrangian simulations, Progress in Oceanography, 199, 102 697, 2021.

890 Miller, D., Poucher, S., and Coiro, L.: Determination of lethal dissolved oxygen levels for selected marine and estuarine fishes, crustaceans, and a bivalve, Marine Biology, 140, 287–296, 2002.

Naqvi, S. W. A.: Deoxygenation in marginal seas of the Indian ocean, Frontiers in Marine Science, 8, 624 322, 2021.

Nicholas, T., Busecke, J., and Abernathey, R.: xGCM: Staggered Grids, Topologies, and Ufuncs in Python, in: 103rd AMS Annual Meeting, AMS, 2023.

895 O'Neill, B. C., Tebaldi, C., Van Vuuren, D. P., Eyring, V., Friedlingstein, P., Hurtt, G., Knutti, R., Kriegler, E., Lamarque, J.-F., Lowe, J., et al.: The scenario model intercomparison project (ScenarioMIP) for CMIP6, Geoscientific Model Development, 9, 3461–3482, 2016.

Oschlies, A., Schulz, K. G., Riebesell, U., and Schmittner, A.: Simulated 21st century's increase in oceanic suboxia by CO2-enhanced biotic carbon export, Global Biogeochemical Cycles, 22, 2008.

Oschlies, A., Brandt, P., Stramma, L., and Schmidtko, S.: Drivers and mechanisms of ocean deoxygenation, Nature Geoscience, 11, 467–473,
900 2018.

Paulmier, A. and Ruiz-Pino, D.: Oxygen minimum zones (OMZs) in the modern ocean, Progress in Oceanography, 80, 113–128, 2009.

Pedlosky, J.: Eastern boundary ventilation and the structure of the thermocline, Journal of physical oceanography, 13, 2038–2044, 1983.

Phillips, H. E., Tandon, A., Furue, R., Hood, R., Ummenhofer, C. C., Benthuysen, J. A., Menezes, V., Hu, S., Webber, B., Sanchez-Franks, A., et al.: Progress in understanding of Indian Ocean circulation, variability, air–sea exchange, and impacts on biogeochemistry, Ocean Science, 17, 1677–1751, 2021.

905 Piontkovski, S. and Al-Oufi, H.: The Omani shelf hypoxia and the warming Arabian Sea, International Journal of Environmental Studies, 72, 256–264, 2015.

Prince, E. D. and Goodyear, C. P.: Hypoxia-based habitat compression of tropical pelagic fishes, Fisheries Oceanography, 15, 451–464, 2006.

Queste, B. Y., Vic, C., Heywood, K. J., and Piontkovski, S. A.: Physical controls on oxygen distribution and denitrification potential in the
910 north west Arabian Sea, Geophysical Research Letters, 45, 4143–4152, 2018.

Rahmstorf, S., Box, J. E., Feulner, G., Mann, M. E., Robinson, A., Rutherford, S., and Schaffernicht, E. J.: Exceptional twentieth-century slowdown in Atlantic Ocean overturning circulation, Nature climate change, 5, 475–480, 2015.

Resplandy, L.: Will ocean zones with low oxygen levels expand or shrink?, 2018.

Resplandy, L., Lévy, M., Bopp, L., Echevin, V., Pous, S., Sarma, V., and Kumar, D.: Controlling factors of the oxygen balance in the Arabian
915 Sea's OMZ, Biogeosciences, 9, 5095–5109, 2012.

Rhein, M., Stramma, L., and Plähn, O.: Tracer signals of the intermediate layer of the Arabian Sea, Geophysical research letters, 24, 2561–2564, 1997.

Rixen, T., Cowie, G., Gaye, B., Goes, J., do Rosário Gomes, H., Hood, R. R., Lachkar, Z., Schmidt, H., Segschneider, J., and Singh, A.: Present past and future of the OMZ in the northern Indian Ocean, Biogeosci. Discuss, 10, 2020.

920 Roxy, M. K., Ritika, K., Terray, P., and Masson, S.: The curious case of Indian Ocean warming, Journal of Climate, 27, 8501–8509, 2014.

Roy, A.: Blue economy in the Indian Ocean: Governance perspectives for sustainable development in the region, ORF Occasional Paper, 181, 2019.

Schmidt, H., Getzlaff, J., Löptien, U., and Oschlies, A.: Causes of uncertainties in the representation of the Arabian Sea oxygen minimum zone in CMIP5 models, Ocean Science, 17, 1303–1320, 2021.

925 Schmidtko, S., Stramma, L., and Visbeck, M.: Decline in global oceanic oxygen content during the past five decades, Nature, 542, 335–339, 2017.

Schott, F. A., Dengler, M., and Schoenefeldt, R.: The shallow overturning circulation of the Indian Ocean, Progress in oceanography, 53, 57–103, 2002.

Schott, F. A., Xie, S.-P., and McCreary Jr, J. P.: Indian Ocean circulation and climate variability, Reviews of Geophysics, 47, 2009.

930 Schupfner, M., Wieners, K.-H., Wachsmann, F., Steger, C., Bittner, M., Jungclaus, J., Früh, B., Pankatz, K., Giorgetta, M., Reick, C., Legutke, S., Esch, M., Gayler, V., Haak, H., de Vrese, P., Raddatz, T., Mauritsen, T., von Storch, J.-S., Behrens, J., Brovkin, V., Claussen, M., Crueger, T., Fast, I., Fiedler, S., Hagemann, S., Hohenegger, C., Jahns, T., Kloster, S., Kinne, S., Lasslop, G., Kornblueh, L., Marotzke, J., Matei, D., Meraner, K., Mikolajewicz, U., Modali, K., Müller, W., Nabel, J., Notz, D., Peters, K., Pincus, R., Pohlmann, H., Pongratz, J., Rast, S., Schmidt, H., Schnur, R., Schulzweida, U., Six, K., Stevens, B., Voigt, A., and Roeckner, E.: DKRZ MPI-ESM1.2-HR model
935 output prepared for CMIP6 ScenarioMIP, https://doi.org/10.22033/ESGF/CMIP6.2450, 2019.

Seland, Ø., Bentsen, M., Olivié, D., Toniazzo, T., Gjermundsen, A., Graff, L. S., Debernard, J. B., Gupta, A. K., He, Y.-C., Kirkevåg, A., et al.: Overview of the Norwegian Earth System Model (NorESM2) and key climate response of CMIP6 DECK, historical, and scenario simulations, Geoscientific Model Development, 13, 6165–6200, 2020.

Seland, y., Bentsen, M., Olivè, D. J. L., Toniazzo, T., Gjermundsen, A., Graff, L. S., Debernard, J. B., Gupta, A. K., He, Y., Kirkevåg,
940 A., Schwinger, J., Tjiputra, J., Aas, K. S., Bethke, I., Fan, Y., Griesfeller, J., Grini, A., Guo, C., Ilicak, M., Karset, I. H. H., Landgren,

O. A., Liakka, J., Moseid, K. O., Nummelin, A., Spensberger, C., Tang, H., Zhang, Z., Heinze, C., Iversen, T., and Schulz, M.: NCC NorESM2-LM model output prepared for CMIP6 CMIP, https://doi.org/10.22033/ESGF/CMIP6.502, 2019a.

Seland, y., Bentsen, M., Oliviè, D. J. L., Toniazzo, T., Gjermundsen, A., Graff, L. S., Debernard, J. B., Gupta, A. K., He, Y., Kirkevåg, A., Schwinger, J., Tjiputra, J., Aas, K. S., Bethke, I., Fan, Y., Griesfeller, J., Grini, A., Guo, C., Ilicak, M., Karset, I. H. H., Landgren,

945   O. A., Liakka, J., Moseid, K. O., Nummelin, A., Spensberger, C., Tang, H., Zhang, Z., Heinze, C., Iversen, T., and Schulz, M.: NCC NorESM2-LM model output prepared for CMIP6 ScenarioMIP, https://doi.org/10.22033/ESGF/CMIP6.604, 2019b.

Sen Gupta, A., McGregor, S., Van Sebille, E., Ganachaud, A., Brown, J. N., and Santoso, A.: Future changes to the Indonesian Throughflow and Pacific circulation: The differing role of wind and deep circulation changes, Geophysical Research Letters, 43, 1669–1678, 2016.

Sharma, S., Ha, K.-J., Yamaguchi, R., Rodgers, K. B., Timmermann, A., and Chung, E.-S.: Future Indian Ocean warming patterns, Nature

950   Communications, 14, 1789, 2023.

Sheehan, P. M., Webber, B. G., Sanchez-Franks, A., Matthews, A. J., Heywood, K. J., and Vinayachandran, P.: Injection of oxygenated Persian Gulf Water into the southern Bay of Bengal, Geophysical Research Letters, 47, e2020GL087 773, 2020.

Shrikumar, A., Lawrence, R., and Casciotti, K. L.: PYOMPA version 0.3, Authorea Preprints, 2022.

Sofianos, S. S. and Johns, W. E.: Observations of the summer Red Sea circulation, Journal of Geophysical Research: Oceans, 112, 2007.

955 Sprintall, J. and Tomczak, M.: On the formation of Central Water and thermocline ventilation in the southern hemisphere, Deep Sea Research Part I: Oceanographic Research Papers, 40, 827–848, 1993.

Sprintall, J., Wijffels, S. E., Molcard, R., and Jaya, I.: Direct estimates of the Indonesian Throughflow entering the Indian Ocean: 2004–2006, Journal of Geophysical Research: Oceans, 114, 2009.

Stellema, A., Sen Gupta, A., and Taschetto, A. S.: Projected slow down of South Indian Ocean circulation, Scientific reports, 9, 1–15, 2019.

960 Stramma, L., Johnson, G. C., Sprintall, J., and Mohrholz, V.: Expanding oxygen-minimum zones in the tropical oceans, science, 320, 655–658, 2008.

Stramma, L., Prince, E. D., Schmidtko, S., Luo, J., Hoolihan, J. P., Visbeck, M., Wallace, D. W., Brandt, P., and Körtzinger, A.: Expansion of oxygen minimum zones may reduce available habitat for tropical pelagic fishes, Nature Climate Change, 2, 33–37, 2012.

Sun, S. and Thompson, A. F.: Centennial changes in the Indonesian Throughflow connected to the Atlantic meridional overturning circulation:

965   The ocean's transient conveyor belt, Geophysical Research Letters, 47, e2020GL090 615, 2020.

Tachiiri, K., Abe, M., Hajima, T., Arakawa, O., Suzuki, T., Komuro, Y., Ogochi, K., Watanabe, M., Yamamoto, A., Tatebe, H., Noguchi, M. A., Ohgaito, R., Ito, A., Yamazaki, D., Ito, A., Takata, K., Watanabe, S., and Kawamiya, M.: MIROC MIROC-ES2L model output prepared for CMIP6 ScenarioMIP, https://doi.org/10.22033/ESGF/CMIP6.936, 2019.

Takano, Y., Ito, T., and Deutsch, C.: Projected centennial oxygen trends and their attribution to distinct ocean climate forcings, Global

970   Biogeochemical Cycles, 32, 1329–1349, 2018.

Talley, L. D.: Descriptive physical oceanography: an introduction, Academic press, 2011.

Tang, Y., Rumbold, S., Ellis, R., Kelley, D., Mulcahy, J., Sellar, A., Walton, J., and Jones, C.: MOHC UKESM1.0-LL model output prepared for CMIP6 CMIP, https://doi.org/10.22033/ESGF/CMIP6.1569, 2019.

Tomczak, M. and Large, D. G.: Optimum multiparameter analysis of mixing in the thermocline of the eastern Indian Ocean, Journal of

975   Geophysical Research: Oceans, 94, 16 141–16 149, 1989.

Vallivattathillam, P., Lachkar, Z., and Le´vy, M.: Shrinking of the Arabian Sea oxygen minimum zone with climate change projected with a downscaled model, Frontiers in Marine Science, 10, 1123 739, 2023.

Vaquer-Sunyer, R. and Duarte, C. M.: Thresholds of hypoxia for marine biodiversity, Proceedings of the National Academy of Sciences, 105, 15 452–15 457, 2008.

980 Wieners, K.-H., Giorgetta, M., Jungclaus, J., Reick, C., Esch, M., Bittner, M., Gayler, V., Haak, H., de Vrese, P., Raddatz, T., Mauritsen, T., von Storch, J.-S., Behrens, J., Brovkin, V., Claussen, M., Crueger, T., Fast, I., Fiedler, S., Hagemann, S., Hohenegger, C., Jahns, T., Kloster, S., Kinne, S., Lasslop, G., Kornblueh, L., Marotzke, J., Matei, D., Meraner, K., Mikolajewicz, U., Modali, K., Müller, W., Nabel, J., Notz, D., Peters, K., Pincus, R., Pohlmann, H., Pongratz, J., Rast, S., Schmidt, H., Schnur, R., Schulzweida, U., Six, K., Stevens, B., Voigt, A., and Roeckner, E.: MPI-M MPIESM1.2-LR model output prepared for CMIP6 ScenarioMIP, https://doi.org/10.22033/ESGF/CMIP6.793,
985 2019a.

Wieners, K.-H., Giorgetta, M., Jungclaus, J., Reick, C., Esch, M., Bittner, M., Legutke, S., Schupfner, M., Wachsmann, F., Gayler, V., Haak, H., de Vrese, P., Raddatz, T., Mauritsen, T., von Storch, J.-S., Behrens, J., Brovkin, V., Claussen, M., Crueger, T., Fast, I., Fiedler, S., Hagemann, S., Hohenegger, C., Jahns, T., Kloster, S., Kinne, S., Lasslop, G., Kornblueh, L., Marotzke, J., Matei, D., Meraner, K., Mikolajewicz, U., Modali, K., Müller, W., Nabel, J., Notz, D., Peters, K., Pincus, R., Pohlmann, H., Pongratz, J., Rast, S., Schmidt, H.,
990 Schnur, R., Schulzweida, U., Six, K., Stevens, B., Voigt, A., and Roeckner, E.: MPI-M MPIESM1.2-LR model output prepared for CMIP6 CMIP, https://doi.org/10.22033/ESGF/CMIP6.742, 2019b.

Zhuang, J., Dussin, R., Huard, D., Bourgault, P., Banihirwe, A., Hamman, J., Jüling, A., Filipe, Rondeau, G., Rasp, S., and et al.: pangeo-data/xESMF: v0.5.2, https://doi.org/10.5281/zenodo.4464833, 2021.